UNIVERSIDADE FEDERAL DO RIO GRANDE DO SUL
ESCOLA DE ENGENHARIA
PROGRAMA DE PÓS-GRADUAÇÃO EM ENGENHARIA ELÉTRICA

MAURÍCIO SPIAZZI RICHTER

VISION-BASED CONTROL OF A DIFFERENTIAL-ALGEBRAIC *QUATERNION* CAMERA MODEL

Porto Alegre
2021

MAURÍCIO SPIAZZI RICHTER

VISION-BASED CONTROL OF A DIFFERENTIAL-ALGEBRAIC *QUATERNION* CAMERA MODEL

Thesis presented to Programa de Pós-Graduação em Engenharia Elétrica of Universidade Federal do Rio Grande do Sul in partial fulfillment of the requirements for the degree of Master in Electrical Engineering.
Area: Control and Automation

ADVISOR: Prof. Dr. Aurélio Tergolina Salton

Porto Alegre
2021

MAURÍCIO SPIAZZI RICHTER

VISION-BASED CONTROL OF A DIFFERENTIAL-ALGEBRAIC *QUATERNION* CAMERA MODEL

This thesis was considered adequate for obtaining the degree of Master in Electrical Engineering and approved in its final form by the Advisor and the Examination Committee.

Advisor: _____
Prof. Dr. Aurélio Tergolina Salton, UFRGS
Doctor by the University of Newcastle - Newcastle, Australia

Examination Committee:

Prof. Dr. Daniel Ferreira Coutinho, UFSC
Doctor by Universidade Federal de Santa Catarina – Florianópolis, Brazil

Prof. Dr. Rafael da Silveira Castro, PUCRS
Doctor by Universidade Federal do Rio Grande do Sul – Porto Alegre, Brazil

Prof. Dr. Jeferson Vieira Flores, UFRGS
Doctor by Universidade Federal do Rio Grande do Sul – Porto Alegre, Brazil

Coordinator of PPGEE: _____
Prof. Dr. Sérgio Luís Haffner

Porto Alegre, May 28^{th} 2021.

DEDICATION

To my wife Liciane, my partner in life.
And to my parents, Carlos and Magali, for the unconditional support and care.

ACKNOWLEDGEMENTS

I would like to express my deepest gratitude to my wife Liciane, and my parents, Carlos and Magali, for the tireless support in every way possible over the whole process that resulted in this work.

Special thanks also to my sister, Letícia, whose incentive comes always as a relieving feeling to go ahead and do my best.

Thanks to Prof. Dr. Aurélio Salton, for all the high quality technical advice that made this project possible, and for valuing my efforts during the process.

Thanks to the secretary of PPGEE-UFRGS, Miriam Rosek, for solving absolutely every issue that was on her hands.

To the PPGEE-UFRGS, for the opportunity of acquiring such important qualification and experience.

To AEL Sistemas, for encouraging, valuing and providing means to make this personal and professional growth viable.

Also, my sincere thanks to my friends and former classmates, Bruno and Rodrigo, who will certainly always have a part in all my professional achievements.

And, of course, to all my family, especially my beloved grandparents, who are always part of all my projects, directly or not.

ABSTRACT

This work deals with the image-based feedback control of a camera, providing an optimization-based control design method for a controller that positions the projection of an external point (feature) at a specified display coordinate. Working with a Differential-Algebraic Representation (DAR) of the camera dynamics modeled in terms of quaternions, a static output feedback (SOF) controller that uses the error between the desired and current image is determined to generate a torque input for the system. From the Lyapunov method for stability analysis, the problem is converted into an optimization problem subject to constraints in the form of Bilinear Matrix Inequalities (BMI), which is solved through an iterative process. The results with DAR are compared to a similar process using a Quasi-Linear Parameter-Varying (Quasi-LPV) representation, which is developed in parallel along the text. Numerical results are provided to demonstrate the practicability of the method and show that a feasible solution achieves the objective of making the error asymptotically approach zero.

Keywords: Nonlinear Systems, Visual-Based Rotation Control, Differential Algebraic Representation, Linear Matrix Inequalities, Static Output Feedback.

RESUMO

Este trabalho lida com controle baseado em realimentação da imagem de uma câmera, fornecendo um método de projeto de controlador baseado em otimização, para um controlador que posiciona a projeção de um ponto externo em uma coordenada de exibição especificada. Trabalhando com uma Representação Diferencial Algébrica (DAR) da dinâmica da câmera modelada em termos de quaternions, um controlador com realimentação estática de saída (SOF) que usa o erro entre a imagem desejada e a atual é determinado para gerar uma entrada de torque para o sistema. A partir do método de análise de estabilidade de Lyapunov, o problema é convertido em um problema de otimização sujeito a restrições sob a forma de Desigualdades Matriciais Bilineares (BMI), o qual é resolvido através de um processo iterativo. Os resultados com DAR são comparados a um processo semelhante usando uma representação de Variação Paramétrica Quase Linear (Quasi-LPV), a qual é desenvolvida em paralelo ao longo do texto. Resultados numéricos são fornecidos para demonstrar a praticidade do método e mostrar que uma solução viável atinge o objetivo de fazer com que o erro se aproxime assintoticamente a zero.

Palavras-chave: Sistemas não lineares, Controle de Rotação Baseado em Visão, Representação Algébrica Diferencial, Desigualdades Matriciais Lineares, Realimentação Estática de Saída.

LIST OF FIGURES

LIST OF ABBREVIATIONS

BMI	Bilinear Matrix Inequalities
DAR	Differential Algebraic Representation
DoI	Domain of Interest
LMI	Linear Matrix Inequalities
LPV	Linear Parameter-Varying
OP	Optimization Problem
PPGEE	*Programa de Pós-Graduação em Engenharia Elétrica*
RoA	Region of Attraction
SOF	Static Output Feedback

CONTENTS

1 INTRODUCTION

1.1 Motivation and Literature Review

The rigid-body rotational control is a research topic highly motivated by the aerospace sector for the attitude control of aircraft, quadrotors and spacecraft (CHATURVEDI; SANYAL; MCCLAMROCH, 2011), with some of the works making use of the *quaternion* angular representation (MAYHEW; SANFELICE; TEEL, 2011; LEE, 2011; SALTON *et al.*, 2017). Nevertheless, several other applications can be made possible with the development of strategies focused on solving this control problem, such as robotic manipulators (SARAIVA, 2019) or even for the entertainment sector, with virtual reality motion simulators. Having this context in mind, another wide field of study relates to camera orientation control (HU *et al.*, 2009; GLEICHER; WITKIN, 1992; MAHONY; HAMEL, 2005), having applications from sports events broadcasting to public security.

The present work aims at developing a vision-based control for the rotation of a camera, with the objective of positioning the image projection of light emitting points (called *features*) on a desired coordinate of the display. For that, the pinhole camera model is used for image formation (MA *et al.*, 2004; HU *et al.*, 2009) and the control strategy is intended to find an optimal static output feedback (SOF) gain for the closed-loop system.

The nonlinear nature of the system's dynamics enhances the complexity of the problem, requiring an adequate representation of its differential equations. For that, *Quasi-Linear Parameter-Varying (Quasi-LPV)* (HUANG; JADBABAIE, 1999; ROBLES; SALA; BERNAL, 2019) and *Differential Algebraic Representation (DAR)* (COUTINHO *et al.*, 2004; TROFINO; DEZUO, 2014) are used. To tackle the problem effectively, both state feedback (SARAIVA, 2019; SALTON *et al.*, 2017) and output feedback (CASTRO, 2019) control strategies for dynamic nonlinear systems were reviewed and served as a basis for the development of this work.

1.2 Dissertation Contribution

The main objective and contribution of this dissertation is to provide a systematic method for finding a static output feedback control law that stabilizes, using the image

output and the rotation speed, a closed-loop rigid-body dynamic system with *quaternions* representing the rotation of a camera, with the purpose of displaying a *feature* on a desired position of the projected image.

To achieve this objective, state-space models have been obtained using a differential algebraic representation (DAR), containing adequate output equations for output feedback purposes. A Quasi-LPV representation of the same system has also been obtained in order to compare both the accomplishment of the objective and some performance characteristics using one representation or the other.

Using the image error as feedback for the SOF control design, combined with the angular velocity, eliminates the need for having to sense the angular position directly, which is desirable considering it would be an additional quantity to be measured, one that could increase significantly the complexity of the control. The angular velocity, however, can usually be measured more efficiently with less complexity regarding implementation.

While guaranteeing closed-loop stability, it was necessary to design a controller that also maximizes the region of attraction estimate of the system states' initial conditions, based on a predefined maximum desired domain. With the static output feedback controller design resulting in a non-convex optimization problem subject to BMI restrictions, an iterative optimization technique has been applied so it was possible to transform it in a convex optimization problem with LMI restrictions. Performance constraints for exponential decay rate and oscillation reduction have also been added and evaluated in both representations as an extension of the main problem solution.

The research developed and presented in this dissertation has originated the following paper, submitted to the Brazilian Symposium on Automation Intelligence (SBAI) 2021:

- RICHTER, M. S.; SALTON, A. T. Static output feedback control for the rotation of a 2-DOF differential-algebraic quaternion camera.

1.3 Text Outline

The dissertation is organized as follows. In Chapter 2 some background concepts and definitions are presented, including rotation in terms of quaternions, the image formation process for the projection of external points and stability analysis based on matrix inequalities, as well as important mathematical tools that are used throughout the text. In Chapter 3, a rigid-body dynamic rotation model using quaternions is presented in terms of differential equations, where the output of the system is also defined adequately for the proposed work. Quasi-LPV and DAR state-space representations for the system are then defined, whose resulting matrices are applied to the closed-loop analysis. In Chapter 4, the control design problem is addressed as an optimization problem to be solved considering both model representations, Quasi-LPV and DAR, for a predefined domain of interest. A polytopic approach that serves as a basis for the BMI/LMI stability conditions

is presented for addressing varying parameters inside state-space matrices. The solutions developed considering performance extensions for decay rate and reduced oscillation are also explained. In Chapter 5, simulation results are presented and analyzed to verify the achieved solution methods. Finally, in Chapter 6, concluding remarks and suggestions for future works are presented.

2 PRELIMINARIES

2.1 Quaternions and Inertial Frames

The orientation of a rigid body can be expressed in terms of *quaternions* (MAYHEW; SANFELICE; TEEL, 2011; SPRING, 1986; DE FARIA *et al.*, 2016), which are hypercomplex numbers, or quadruples of real numbers $q = (\eta, \epsilon_x, \epsilon_y, \epsilon_z)$ forming a four-dimensional real vector space $\mathbb{H}$ (named after their creator William Hamilton) (KRISHNASWAMI; SACHDEV, 2016).

The *quaternions* can, then, be written as $q = \eta + \epsilon_x\hat{i} + \epsilon_y\hat{j} + \epsilon_z\hat{k} = \eta + \vec{\epsilon}$, where η is called the "scalar" part and $\vec{\epsilon} = \epsilon$ the "vectorial" part of q (KRISHNASWAMI; SACHDEV, 2016). Considering a *unit quaternion* has norm equal to 1 (DAM; KOCH; LILLHOLM, 1998), it is possible to establish the relationship between η and ϵ according to equation (1).

$$\eta^2 + \epsilon^\intercal\epsilon = 1 \tag{1}$$

In addition to that, according to (KRISHNASWAMI; SACHDEV, 2016), similarly to Euler's formula $e^{i\psi} = \cos(\psi) + i\sin(\psi)$ for unit complex numbers, *unit quaternions* can be expressed by (2).

$$q = \cos(\psi/2) + \vec{r}\sin(\psi/2) \tag{2}$$

From that, it is possible to represent the *quaternions* as follows:

$$q = \begin{bmatrix} \cos(\frac{\psi}{2}) \\ \vec{r}\sin(\frac{\psi}{2}) \end{bmatrix} = \begin{bmatrix} \eta \\ \epsilon \end{bmatrix} = \begin{bmatrix} \eta \\ \epsilon_x \\ \epsilon_y \\ \epsilon_z \end{bmatrix} \tag{3}$$

where $\eta \in \mathbb{R}$, $\epsilon \in \mathbb{R}^3$, $\psi \in \mathbb{R}$ is the rotation angle $[rad]$ and $\vec{r} \in \mathbb{R}^3$ describes the rotation axis and its direction (by using the right-hand rule).

To establish the references for the angular movement of the camera, two Inertial Frames are defined:

- *Reference frame* $\bar{\mathcal{F}}$: representing the desired orientation of the camera, in which the $\bar{Z}$ axis points to where the camera should point so that the *feature* would be at the desired position on the projected image. Supposing one is "looking" towards $\bar{Z}$, $\bar{X}$ and $\bar{Y}$ are orthogonal axes, pointing to the right and up, respectively.

- *Body frame* $\mathcal{F}$: representing the camera frame, with the Z axis along a line on the direction the camera is pointing to, X to the right of the camera and Y pointing up.

Since this work does not deal with any camera translation, the *body frame* is considered to be positioned at the origin of the *reference frame*.

In this context, a rotation matrix in terms of a *quaternion* can be derived relating one frame to the other. The rotation matrix defined as $R(q)$, which is equivalent to a set of 3 subsequent Euler angle rotations, will then represent the necessary rotation for the camera to have the desired orientation, i.e., to rotate the body through an angle ψ about the unit vector $\vec{r}$ (SPRING, 1986).

By introducing the half-angle trigonometric functions to the rotating operator (using Rodrigues formula) (SHAH, 1997; MAYHEW; SANFELICE; TEEL, 2011; KRISHNASWAMI; SACHDEV, 2016), the matrix in terms of *quaternions* representing a rotation ψ about the $\vec{r}$ axis and relating the *body frame* to the *reference frame* can finally be obtained in (4) (MARKLEY; CRASSIDIS, 2014).

$$R(q) = I - 2\eta S(\epsilon) + 2S(\epsilon)^2 \tag{4}$$

where $R(q) \in SO(3)$ (group of all rotations about the origin of the 3D Euclidean space) and $S(\cdot)$ represents the cross-product in matrix form[1].

2.2 Image Formation

To begin with, the pinhole camera model is presented, which is used in this work as a basis for the image projection calculations. The main aspect of this model is that it considers the aperture of a thin lens as an infinitesimal hole through which all light rays are forced to pass, remaining therefore undeflected (MA *et al.*, 2004). Due to that, the only external light emitting points that contribute to the projection of each $\{\hat{x}, \hat{y}\}$ position on the display lie on a line going through the center of the lens and reaching the image plane behind it.

Spatially, this relation between an external point $\{\mu_x, \mu_y, \mu_z\}$ and the position where the line intersects the image plane can be seen in figure 1 and represented mathematically

[1] In matrix form, the cross-product $\vec{v} \times \vec{w}$ can be expressed by:

$$S(\vec{v})\vec{w} = \begin{bmatrix} 0 & -v_3 & v_2 \\ v_3 & 0 & -v_1 \\ -v_2 & v_1 & 0 \end{bmatrix} \begin{bmatrix} w_1 \\ w_2 \\ w_3 \end{bmatrix} \tag{5}$$

through equation (6) (MA *et al.*, 2004; SHAH, 1997). Note, however, that the original equation has a minus sign in front of f, which is, instead, hereby assumed to be positive. This is done to eliminate the image flipping effect, meaning therefore that the image plane is considered to be in front of the lens ("frontal" pinhole model), inverting the direction of the axis perpendicular to it (MA *et al.*, 2004).

$$x_{dist} = f\frac{\mu_x}{\mu_z} \qquad y_{dist} = f\frac{\mu_y}{\mu_z} \tag{6}$$

where f is the focal length of the camera in units of distance.

Figure 1 – "Frontal" pinhole imaging model.

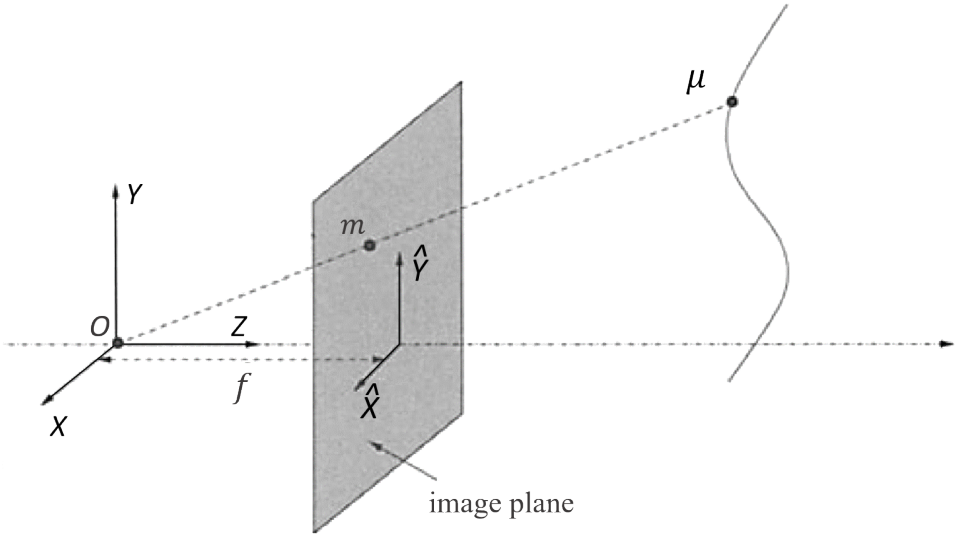

Source: adapted from MA *et* al, 2004

To provide a sufficient description of the imaging process using the pinhole model and how the equations that derive from it are applied to the problem in scope, it is useful at this point to briefly explain the homogeneous coordinates. Following, the definition, taken from (GRAUSTEIN, 1930):

Definition 2.1. *Homogeneous Coordinates* (p_1, p_2, p_3) *of the finite point* (z_1, z_2) *are any three numbers* p_1, p_2, p_3 *for which*

$$\frac{p_1}{p_3} = z_1, \qquad \frac{p_2}{p_3} = z_2 \tag{7}$$

Taking that into account, a point has an infinite set of homogenous coordinates proportional to the third coordinate, being represented by $\{\lambda z_1, \lambda z_2, \lambda\}$, where λ can assume any value. Analogously to the illustration in figure 1 for the image plane, a 2D point can be seen as the intersection of a line from the origin to the infinity with a plane spaced λ from the origin. A particular case is for instance when the depth $\lambda = 1$, which makes, as a

reference to (7), $p_1 = z_1$ and $p_2 = z_2$. Additionally, extending this definition to n dimensions, every set of coordinates can be represented by an $(n + 1)$ number of homogeneous coordinates.

This system of coordinates also provides a useful representation for points at infinity $\{z_1, z_2, 0\}$ (GRAUSTEIN, 1930) as well as facilitates some transformations (e.g., translation, rotation and scaling) to be done using operations with matrices (MA *et al.*, 2004; SHAH, 1997).

From (6) and considering the pixel scaling and translation to the principal point of the display, the image projection of a point can be calculated according to (HU *et al.*, 2009; MA *et al.*, 2004):

$$m = \underbrace{\begin{bmatrix} f_x & f_\theta & o_x \\ 0 & f_y & o_y \\ 0 & 0 & 1 \end{bmatrix}}_{K_c} \mu_n \tag{8}$$

where $m = [\hat{x} \quad \hat{y} \quad 1]^\intercal$ establishes the image projection coordinates, $\mu_n \in \mathbb{R}^3$ is the normalized point in relation to the body (camera) frame, in homogeneous coordinates, and $K_c \in \mathbb{R}^{3\times3}$ is the intrinsic parameters matrix.

The intrinsic parameters concatenated in matrix K_c are parameters dependent on the camera, based only on its calibration or physical characteristics, being those (HU *et al.*, 2009; MA *et al.*, 2004):

- $o_x, o_y \in \mathbb{R}$ - pixel coordinates of the principal point (image center);
- $f_x \in \mathbb{R} : f_x = \rho_x$ - where ρ_x is the size of unit length in horizontal pixels;
- $f_y \in \mathbb{R} : f_y = \frac{\rho_y}{\sin(\theta)}$ - where ρ_y is the size of unit length in vertical pixels and θ is the skew angle between camera axes;
- $f_\theta \in \mathbb{R} : f_\theta = -\rho_x \cot(\theta)$ - where ρ_x is the size of unit length in horizontal pixels and θ is the skew angle between camera axes.

Considering also the rotation of the point in matrix form (no translation treated), to modify the reference of μ from the body frame to the reference frame, the image projection equation becomes (MA *et al.*, 2004):

$$\lambda m = K_c R(q) \mu_0 \tag{9}$$

where $\mu_0 \in \mathbb{R}$ is the point in relation to the reference frame, in homogeneous coordinates and $\lambda \in \mathbb{R}$ is the depth of the rotated point in relation to the camera frame.

2.2.1 Features

The light emitting points which are projected on the camera image are called *features*. It is important to mention that the control applied on the camera is based on the relative orientation between the orientation of the camera and the *feature*. The *feature's* spatial coordinates $\{\mu_x, \mu_y, \mu_z\}$ in relation to the *body frame* correspond to the current image

being displayed when the rotation matrix is the Identity, i.e., with no rotation applied. The feature μ can, then, be represented by equation (10):

$$\mu = \begin{bmatrix} \mu_x & \mu_y & \mu_z \end{bmatrix}^\intercal \rightarrow \mu_n = \begin{bmatrix} \mu_x/\mu_z & \mu_y/\mu_z & 1 \end{bmatrix}^\intercal \tag{10}$$

Note that the point coordinates were normalized so that the third term ($\bar{Z}$ axis) is equal to 1. This is due to the fact that for the projected image, the original and the normalized coordinates are equivalent (see the definition of homogeneous coordinates in section 2.2), but the output of the image formation equation only represents the exact pixel coordinates on the screen in case this "depth" term is 1 (see equation (9)).

2.3 Lyapunov Stability using Matrix Inequalities

The study of stability of equilibrium points is a matter of huge interest when dealing with the design of nonlinear control systems, and this is no different in the scope of this work. Considering that, the concept of Lyapunov stability turns out to be useful in this context, providing criteria to analyze objectively such characteristic. As explained in (KHALIL, 2002), "Lyapunov stability theorems give sufficient conditions for stability, asymptotic stability, and so on."

In light of this, the following definition taken from (KHALIL, 2002) is presented, precisely defining stability for an equilibrium point at the origin, which can be extended to all equilibrium points with no loss of generality:

Definition 2.2. *Consider the autonomous system*

$$\dot{x} = f(x) \tag{11}$$

where $f : \mathcal{X} \rightarrow \mathbb{R}^n$ is a local Lipschitz map from a domain $\mathcal{X} \subset \mathbb{R}^n$ into $\mathbb{R}^n$.
Suppose $\bar{x} \in \mathcal{X}$ is an equilibrium point of (11) *at the origin of $\mathbb{R}^n$, i.e., $f(\bar{x}) = 0$.*
Then, the equilibrium point $\bar{x} = 0$ is

- *stable if, for each $\epsilon > 0$, there is a $\delta = \delta(\epsilon) > 0$ such that*

$$\|x(0)\| < \delta \Rightarrow \|x(t)\| < \epsilon, \ \forall t \geq 0 \tag{12}$$

- *unstable if it is not stable.*
- *asymptotically stable if it is stable and δ can be chosen such that*

$$\|x(0)\| < \delta \Rightarrow \lim_{t \rightarrow \infty} x(t) = 0 \tag{13}$$

More specifically, the stability problem for rational nonlinear systems in a differential-algebraic representation is addressed by (COUTINHO *et al.*, 2004) and (TROFINO; DEZUO, 2014) (which treats also uncertain parameters in the modelling), presenting sufficient LMI conditions that assure stability of the equilibrium points by applying the Lyapunov theory.

Such matrix inequalities conditions are extensively used in this work, coming as a result of the stability analysis for the control design proposed. However, as it can be verified in the following chapters, the static output feedback applied brings with it an additional problem: considering the way that the matrix inequalities variables become structured, it is not trivial to recover the feedback gain with a simple substitution of variables. Therefore, it becomes necessary to solve directly the BMI that follows from the stability analysis.

The problem of checking the solvability of BMIs is classified as NP-hard (*i.e.,* non-deterministic polynomial-hard), as shown in (TOKER; OZBAY, 1995). This classification comes from the P versus NP problem, an important problem in computer science concerned with the limits of feasible computation (COOK, 2003). The impact, as it is explained in (SADABADI; PEAUCELLE, 2016), is that although BMI solvers exist, they most often fail to provide a solution for SOF problems with BMI restrictions, requiring other indirect methods to be used, such as with iterative LMI heuristics. This is the case of the P-K algorithm used (EL GHAOUI; BALAKRISHNAN, 1994), serving as a successful tool to help finding a feedback gain that satisfies the Lyapunov stability conditions mentioned above.

2.4 Background Mathematical Techniques

Some useful mathematical and algebraic techniques which were taken from (BRIAT, 2015; BOYD; VANDENBERGHE, 2004) are highlighted in this section, serving as important tools to the development of this work.

Lemma 2.1. *(Schur complement) Consider matrices $A \in \mathbb{S}^{n_1}$, $C \in \mathbb{S}^{n_2}$ and $B \in \mathbb{R}^{n_1 \times n_2}$. Then, the following inequalities are equivalent:*

i

$$\begin{bmatrix} A & B \\ B^\intercal & C \end{bmatrix} \succeq 0 \tag{14}$$

ii

$$A \succeq 0 \ \textit{and} \ C - B^\intercal A^{-1} B \succeq 0 \tag{15}$$

iii

$$C \succeq 0 \ \textit{and} \ A - B C^{-1} B^\intercal \succeq 0 \tag{16}$$

Proof can be obtained in (BOYD; VANDENBERGHE, 2004).

Lemma 2.2. *($\mathcal{S}$-procedure) Consider symmetric matrices $P_0, P_1, \ldots, P_m \in \mathbb{R}^{n \times n}$ where*

$$\mathcal{X} = \left\{ x \in \mathbb{R}^n : x^\intercal P_i x \leq 0, \ i = 1, \ldots, m \right\} \tag{17}$$

If there exist scalars $\tau_1, \ldots, \tau_m \geq 0$ *such that*

$$P_0 - \sum_{i=1}^{m} \tau_i P_i \leq 0 \tag{18}$$

then $x^\intercal P_0 x \leq 0 \; \forall \; x \in \mathcal{X}, \; x \neq 0$.

Proof can be obtained in (BOYD; VANDENBERGHE, 2004).

Lemma 2.3. *(Finsler's Lemma) Consider a symmetric matrix* $M \in \mathbb{R}^n$ *and a full-rank matrix* $B \in \mathbb{R}^{m \times n}, m < n$. *Then, the following statements are equivalent:*

i The inequality $x^\intercal M x < 0$ *holds for all* $x \in \mathcal{X}$ *where*

$$\mathcal{X} \coloneqq \{x \in \mathbb{R}^n : Bx = 0, \; x \neq 0\}. \tag{19}$$

ii There exists a symmetric matrix $C \in \mathbb{S}^m$ *such that the inequality*

$$M - B^\intercal C B \preceq 0 \tag{20}$$

holds.

iii There exists a matrix $L \in \mathbb{R}^{m \times n}$ *such that the inequality*

$$M + L^\intercal B + B^\intercal L \preceq 0 \tag{21}$$

holds.

Proof can be obtained in (BOYD *et al.*, 1994).

3 MODELS

3.1 Rigid-Body Dynamic Rotational Model using *Quaternions*

3.1.1 Differential equation model

The rigid-body dynamic model with rotation angle expressed in terms of *quaternions* is described by the set of equations in (22) (CHATURVEDI; SANYAL; MCCLAMROCH, 2011; MARKLEY; CRASSIDIS, 2014):

$$\begin{cases} \dot{\eta} &= -\frac{1}{2}\epsilon^{\intercal}\omega \\ \dot{\epsilon} &= \frac{1}{2}\big(\eta I_3 + S(\epsilon)\big)\omega \\ J\dot{\omega} &= -S(\omega)J\omega + \tau \end{cases} \tag{22}$$

where $\omega \in \mathbb{R}^3$ is the angular velocity $[rad/s]$, $J \in \mathbb{R}^{3x3}$ is a diagonal matrix representing the body moment of inertia around each axis $[kg \cdot m^2]$, $\tau \in \mathbb{R}^3$ is the input torque $[N \cdot m]$ and $S(\cdot)$ represents the cross-product in matrix form.

The open-loop equilibrium points of this system are any η and ϵ representing the *quaternion* with angular velocity $\omega = 0$.

As described in (SALTON *et al.*, 2017), when imposing ϵ to a certain value, η is consequently a result of equation (1). By that, it is possible to eliminate η dynamic behavior equation from the model.

The resulting model to be used is, then, defined by (23).

$$\begin{cases} \dot{\epsilon} &= \frac{1}{2}\big(\eta I_3 + S(\epsilon)\big)\omega \\ J\dot{\omega} &= -S(\omega)J\omega + \tau \end{cases} \tag{23}$$

where, as it is shown on the sections devoted to the state-space modeling of the system, the states will be chosen as ϵ and ω. And, considering η will still appear on the state-space matrices, it will therefore be treated as a time-varying parameter with predefined limits.

3.1.2 Output Definition

Recalling the image formation process described in chapter 2.2, it is straightforward that the output of a camera will be related to its image. Therefore, in order to provide

an adequate signal to serve as a feedback to the system and considering the desired orientation of the camera is such that the feature is projected at a specified position on the display, then the image error is taken as an output of the system.

The image error is defined as the difference between the current or "real" image and the desired image, in terms of pixels along each axis of the display.

Based on the feature image projection process described in (HU *et al.*, 2009), let the vectors $\mu_{\mathcal{F}}$ and $\bar{\mu}_{\bar{\mathcal{F}}}$ represent the current and desired feature's Euclidean coordinates in relation to the body frame $\mathcal{F}$ and reference frame $\bar{\mathcal{F}}$, respectively (inertial frames presented in section 2.1), so that,

$$\begin{aligned} \mu_{\mathcal{F}} &\triangleq \begin{bmatrix} x_\mu & y_\mu & z_\mu \end{bmatrix}^\intercal \\ \bar{\mu}_{\bar{\mathcal{F}}} &\triangleq \begin{bmatrix} \bar{x}_{\bar{\mu}} & \bar{y}_{\bar{\mu}} & \bar{z}_{\bar{\mu}} \end{bmatrix}^\intercal \end{aligned} \tag{24}$$

where $\mu_{\mathcal{F}} \in \mathbb{R}^3$, $\bar{\mu}_{\bar{\mathcal{F}}} \in \mathbb{R}^3$, $x_\mu, y_\mu, z_\mu \in \mathbb{R}$ and $\bar{x}_{\bar{\mu}}, \bar{y}_{\bar{\mu}}, \bar{z}_{\bar{\mu}} \in \mathbb{R}$.

Then, taking into account there is no translation from $\mathcal{F}$ to $\bar{\mathcal{F}}$ (as explained in section 2.1, both frames are positioned at the origin), the geometric relationship between these points can be given by (HU *et al.*, 2009):

$$\mu_{\mathcal{F}} = R(q)\bar{\mu}_{\bar{\mathcal{F}}} \tag{25}$$

where $R(q) \in SO(3)$ represents the orientation of $\bar{\mathcal{F}}$ in relation to $\mathcal{F}$, rotated by ψ as shown in figure 2 (see equation (3)). Note that when the body frame is aligned with the reference frame, $R(q) = I_3$.

Figure 2 – Rotation from body frame to reference frame.

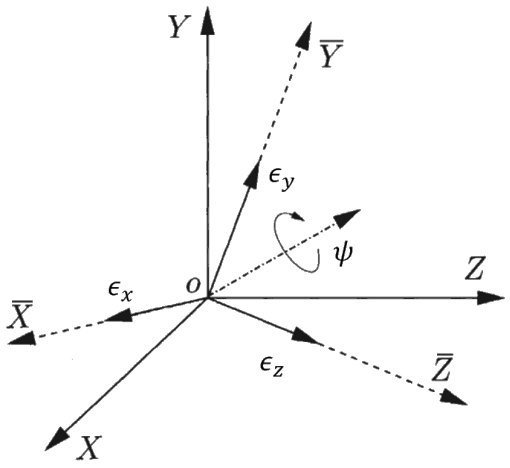

Source: adapted from MA *et* al, 2004

The feature coordinates are normalized so their depth is set as 1, similarly to homogenous coordinates, being defined as:

$$\begin{aligned} \mu_c \triangleq \frac{\mu_{\mathcal{F}}}{z_\mu} &= \begin{bmatrix} \frac{x_\mu}{z_\mu} & \frac{y_\mu}{z_\mu} & 1 \end{bmatrix}^\intercal \Leftrightarrow \mu_{\mathcal{F}} = z_\mu \mu_c \\ \bar{\mu} \triangleq \frac{\bar{\mu}_{\bar{\mathcal{F}}}}{\bar{z}_{\bar{\mu}}} = \begin{bmatrix} \frac{\bar{x}_{\bar{\mu}}}{\bar{z}_{\bar{\mu}}} & \frac{\bar{x}_{\bar{\mu}}}{\bar{z}_{\bar{\mu}}} & 1 \end{bmatrix}^\intercal &\triangleq \begin{bmatrix} a & b & 1 \end{bmatrix}^\intercal \Leftrightarrow \bar{\mu}_{\bar{\mathcal{F}}} = \bar{z}_{\bar{\mu}} \bar{\mu} \end{aligned} \tag{26}$$

which combined with (25) results in the following rotational relationship, adapted from (HU *et al.*, 2009):

$$\mu_c = \frac{\bar{z}_{\bar{\mu}}}{z_\mu} R(q)\bar{\mu} = \gamma R(q)\bar{\mu} \tag{27}$$

where $\gamma \in \mathbb{R}$ is a scaling term based on the actual features' coordinates, interpreted as a depth ratio between them.

Since the feedback control law applied in this work is based on the image error, the scaling term γ in (27) is intentionally $\gamma = 1$ without loss of generality (MA *et al.*, 2004), avoiding unnecessary additional complexity in the image projection error state-space models.

The current and desired feature projections are defined by the vectors:

$$m \triangleq \begin{bmatrix} \hat{x}_m \\ \hat{y}_m \\ 1 \end{bmatrix} \qquad \bar{m} \triangleq \begin{bmatrix} \bar{x}_{\bar{m}} \\ \bar{y}_{\bar{m}} \\ 1 \end{bmatrix} \tag{28}$$

where $m,\ \bar{m} \in \mathbb{R}^3$ are the image projections given by the pinhole camera model (MA *et al.*, 2004; HU *et al.*, 2009) as a result of:

$$\begin{aligned} m &= K_c \mu_c = K_c R(q)\bar{\mu} \\ \bar{m} &= K_c \bar{\mu} \end{aligned} \tag{29}$$

where $K_c \in \mathbb{R}^{3\times 3}$ is the camera intrinsic parameters' matrix described in section 2.2 and, taking into account (27), the current image projection is calculated in terms of the desired feature coordinates and the quaternion rotation between frames.

This brings the image error to be defined as:

$$e = m - \bar{m} = K_c(R(q) - I_3)\bar{\mu} = K_c(-2\eta S(\epsilon) + 2S(\epsilon)^2)\bar{\mu} \tag{30}$$

Another output of the system is the rotation speed ω, which also corresponds to one of the system states. Thinking of ω as a predicted information[2] of the future error (by extrapolation), using it as an additional feedback signal tends to impose to the system an extra – anticipated – control action that can reduce the deviation from the set point, in other words, the overshoot and oscillation. In addition to this, angular velocity sensors are generally low-cost and have a fairly low-complexity on their implementation, as opposed to direct angular position sensing.

Finally, the output of the system can be defined as:

$$y = \begin{bmatrix} e \\ \omega \end{bmatrix} \tag{31}$$

where $y \in \mathbb{R}^6$ is the output of the system, $e \in \mathbb{R}^3$ is the image error and $\omega \in \mathbb{R}^3$ is the rotation speed.

[2]Other signals could have been used for that purpose, e.g. the derivative of the error, but that would bring to the system an undesired complexity, by adding more non-linearity in the feedback loop.

3.2 3D Dynamic Models

Considering the nonlinear nature of the rigid-body rotation dynamics and image projection on the output, in order to address a control design focused on acquiring a stable closed-loop system via matrix inequalities optimization, two state-space representations were used for system modeling: Quasi-LPV and DAR. Through the imposition of further restrictions to the problem, the stabilization problem as well as some performance goals can be addressed by means of linear or bilinear matrix inequalities (LMI/BMI) with both modeling techniques (ROBLES; SALA; BERNAL, 2019; SARAIVA, 2019).

The *Quasi-Linear Parameter-Varying* representation is derived from the LPV modeling, in which the state-space matrices that compose the system are functions of time-varying parameters (KWIATKOWSKI; BOLL; WERNER, 2006). More specifically, the Quasi-LPV approach is characterized by state-space equations in which the system matrices are state-dependent (HUANG; JADBABAIE, 1999; ROBLES; SALA; BERNAL, 2019). This variation on the parameters requires a validity region to be defined for the state variables, which in this case consists of $\{\epsilon \in (-1, 1), \omega \in \mathbb{R}\}$, implying local stability conditions for the analysis.

Another approach to model rational and polynomial nonlinear systems is the *Differential Algebraic Representation*, which as described in (TROFINO; DEZUO, 2014) can be helpful in providing sufficient LMI conditions to design a controller acquiring closed-loop asymptotic stability in a system. As opposed to the quasi-LPV modeling, the DAR succinctly consists in mapping the nonlinearities of a rational function in an additional vector, whose terms are second or higher order groups of the states (TROFINO, 2000; COUTINHO *et al.*, 2004; SALTON *et al.*, 2017; CASTRO, 2019; SARAIVA, 2019). In this representation, an algebraic expression relates the state vector with the nonlinear vector, being that used for both the dynamic of the states and the output if applicable.

Note that to avoid discontinuities in $\eta = 0$, in both model representations the validity region for this variable will be considered $\{\eta \in (0, 1]\}$.

3.2.1 Quasi-LPV 3D Model

The quasi-LPV 3D model is defined by

$$\begin{cases} \dot{x} &= A(x, \eta)x + B\tau \\ y &= C(x, \eta)x \end{cases} \tag{32}$$

where $x \in \mathbb{R}^6$ is the system state vector and $y \in \mathbb{R}^6$ is the output vector. Note that the matrix B is not state-dependent: this is a result of the system modeling and not a characteristic of the representation.

As explained in section 3.1.1, the system states and inputs are characterized by:

$$x = \begin{bmatrix} \epsilon_x \\ \epsilon_y \\ \epsilon_z \\ \omega_x \\ \omega_y \\ \omega_z \end{bmatrix} \quad \tau = \begin{bmatrix} \tau_x \\ \tau_y \\ \tau_z \end{bmatrix} \tag{33}$$

The resulting matrices for the 3D Quasi-LPV representation (which is not unique) are expressed as follows, with $A(x,\eta)$ and B matrices given by

$$A = \begin{bmatrix} 0 & \frac{1}{2}\omega_z & -\frac{1}{2}\omega_y & \frac{1}{2}\eta & 0 & 0 \\ -\frac{1}{2}\omega_z & 0 & \frac{1}{2}\omega_x & 0 & \frac{1}{2}\eta & 0 \\ \frac{1}{2}\omega_y & -\frac{1}{2}\omega_x & 0 & 0 & 0 & \frac{1}{2}\eta \\ 0 & 0 & 0 & 0 & j_x^{-1}(j_y - j_z)w_z & 0 \\ 0 & 0 & 0 & j_y^{-1}(j_z - j_x)w_z & 0 & 0 \\ 0 & 0 & 0 & j_z^{-1}(j_x - j_y)w_y & 0 & 0 \end{bmatrix} \quad B = \begin{bmatrix} & 0_{3x3} & \\ j_x^{-1} & 0 & 0 \\ 0 & j_y^{-1} & 0 \\ 0 & 0 & j_z^{-1} \end{bmatrix}, \tag{34}$$

while by rewriting the error in equation (30) and the rotation speed ω as

$$e = \underbrace{\begin{bmatrix} f_x & f_\theta & o_x \\ 0 & f_y & o_y \\ 0 & 0 & 1 \end{bmatrix}}_{K_c} \underbrace{\begin{bmatrix} -2\epsilon_y^2 - 2\epsilon_z^2 & 2\epsilon_x\epsilon_y + 2\eta\epsilon_z & 2\epsilon_x\epsilon_z - 2\eta\epsilon_y \\ 2\epsilon_x\epsilon_y - 2\eta\epsilon_z & -2\epsilon_x^2 - 2\epsilon_z^2 & 2\epsilon_y\epsilon_z + 2\eta\epsilon_x \\ 2\epsilon_x\epsilon_z + 2\eta\epsilon_y & 2\epsilon_y\epsilon_z - 2\eta\epsilon_x & -2\epsilon_x^2 - 2\epsilon_y^2 \end{bmatrix}}_{(-2\eta S(\epsilon) + 2S(\epsilon)^2)} \underbrace{\begin{bmatrix} a \\ b \\ 1 \end{bmatrix}}_{\bar{\mu}} \tag{35}$$

$$\omega = \begin{bmatrix} 1 & 0 & 0 \\ 0 & 1 & 0 \\ 0 & 0 & 1 \end{bmatrix} \begin{bmatrix} \omega_x \\ \omega_y \\ \omega_z \end{bmatrix}$$

and considering the output $y = \begin{bmatrix} e & \omega \end{bmatrix}^\intercal$ as in (31), matrix $C(x,\eta)$ can be obtained after an algebraic manipulation with $\{\epsilon, \omega\}$ variables in evidence[3].

By that, it can be seen that: $A(x,\eta)$ depends on the rotation speed ω, η and the inertia matrix J (assumed to be constant), B depends only on the inertia matrix J and $C(x,\eta)$, which contains the image-related information, depends on the intrinsic parameters $\{f_x, f_y, f_\theta, o_x, o_y\}$, the desired feature coordinates $\{a, b\}$ and the *quaternion* $\{\eta, \epsilon\}$.

It should be also noted that, in the trivial scenario where the moment of inertia in J is equal for the three axis, i.e. $j_x = j_y = j_z$, then $A(x,\eta)$ is no longer dependent on the ω cross-product, since the bottom-right terms of the matrix are cancelled.

[3]Due to the size of matrix $C(x,\eta)$ and the space limitation, it was chosen to omit the complete matrix.

3.2.2 DAR 3D Model

In accordance with the description given, the DAR 3D model is given by

$$\begin{cases} \dot{x} &= A_1(\eta)x + A_2\xi + B_1\tau \\ 0 &= \Omega_1(x)x + \Omega_2\xi \\ y &= C_1(\eta)x + C_2\pi \\ 0 &= \Pi_1(x)x + \Pi_2\pi \end{cases} \tag{36}$$

where $x \in \mathbb{R}^6$ is the system state vector, $y \in \mathbb{R}^6$ is the output vector, $\xi \in \mathbb{R}^9$ is the nonlinear vector for the rigid-body dynamics and $\pi \in \mathbb{R}^6$ is the nonlinear vector for the output dynamics.

The DAR will be regular if Ω_2 and Π_2 are nonsingular (and therefore invertible). In this case, the original dynamics in (23) and (31) can be recovered by means of

$$\begin{aligned} \dot{x} &= \left(A_1(\eta) - A_2\Omega_2^{-1}\Omega_1(x)\right)x + B_1\tau \\ y &= \left(C_1(\eta) - C_2\Pi_2^{-1}\Pi_1(x)\right)x \end{aligned} \tag{37}$$

Taking as a basis the DAR obtained in (SALTON *et al.*, 2017) for state-feedback and including the output nonlinear terms, the model vectors can be defined as follows:

$$x = \begin{bmatrix} \epsilon_x \\ \epsilon_y \\ \epsilon_z \\ \omega_x \\ \omega_y \\ \omega_z \end{bmatrix} \quad \xi = \begin{bmatrix} \epsilon_x\omega_y \\ \epsilon_x\omega_z \\ \epsilon_y\omega_x \\ \epsilon_y\omega_z \\ \epsilon_z\omega_x \\ \epsilon_z\omega_y \\ \omega_x\omega_y \\ \omega_x\omega_z \\ \omega_y\omega_z \end{bmatrix} \quad \pi = \begin{bmatrix} \epsilon_x^2 \\ \epsilon_y^2 \\ \epsilon_z^2 \\ \epsilon_x\epsilon_y \\ \epsilon_x\epsilon_z \\ \epsilon_y\epsilon_z \end{bmatrix} \quad \tau = \begin{bmatrix} \tau_x \\ \tau_y \\ \tau_z \end{bmatrix} \tag{38}$$

And the resulting matrices for the 3D DAR representation (which is also not unique) are expressed by:

$$\mathrm{A}_1 = \begin{bmatrix} & \frac{1}{2}\eta & 0 & 0 \\ 0_{3x3} & 0 & \frac{1}{2}\eta & 0 \\ & 0 & 0 & \frac{1}{2}\eta \\ 0_{3x3} & & 0_{3x3} & \end{bmatrix} \quad A_2 = \begin{bmatrix} 0 & 0 & 0 & \frac{1}{2} & 0 & -\frac{1}{2} & 0 & 0 & 0 \\ 0 & -\frac{1}{2} & 0 & 0 & \frac{1}{2} & 0 & 0 & 0 & 0 \\ \frac{1}{2} & 0 & -\frac{1}{2} & 0 & 0 & 0 & 0 & 0 & 0 \\ 0 & 0 & 0 & 0 & 0 & 0 & 0 & j_x^{-1}(j_y - j_z) & 0 \\ 0 & 0 & 0 & 0 & 0 & 0 & j_y^{-1}(j_z - j_x) & 0 & 0 \\ 0 & 0 & 0 & 0 & 0 & 0 & j_z^{-1}(j_x - j_y) & 0 & 0 \end{bmatrix}$$

$$\mathbf{B}_1 = \begin{bmatrix} & 0_{3x3} & \\ j_x^{-1} & 0 & 0 \\ 0 & j_y^{-1} & 0 \\ 0 & 0 & j_z^{-1} \end{bmatrix} \quad \Omega_1 = \begin{bmatrix} -\omega_y & 0 & 0 & 0 & 0 & 0 \\ -\omega_z & 0 & 0 & 0 & 0 & 0 \\ 0 & -\omega_x & 0 & 0 & 0 & 0 \\ 0 & -\omega_z & 0 & 0 & 0 & 0 \\ 0 & 0 & -\omega_x & 0 & 0 & 0 \\ 0 & 0 & -\omega_y & 0 & 0 & 0 \\ 0 & 0 & 0 & -\omega_y & 0 & 0 \\ 0 & 0 & 0 & -\omega_z & 0 & 0 \\ 0 & 0 & 0 & 0 & -\omega_z & 0 \end{bmatrix} \quad \Omega_2 = I_{9\times 9}$$

$$C_1 = \begin{bmatrix} 2(f_\theta\eta - o_x b\eta) & 2(o_x a\eta - f_x\eta) & 2(f_x b\eta - f_\theta a\eta) & 0 & 0 & 0 \\ 2(f_y\eta - o_y b\eta) & 2o_y a_\eta & -2f_y a\eta & 0 & 0 & 0 \\ -2b\eta & 2a\eta & 0 & 0 & 0 & 0 \\ 0 & 0 & 0 & 1 & 0 & 0 \\ 0 & 0 & 0 & 0 & 1 & 0 \\ 0 & 0 & 0 & 0 & 0 & 1 \end{bmatrix} \tag{39}$$

$$\mathbf{C}_2 = \begin{bmatrix} -2(o_x - f_\theta b) & -2(o_x - f_x a) & -2(f_x a - f_\theta b) & 2(f_\theta a + f_x b) & 2(f_x + o_x a) & 2(f_\theta + o_x b) \\ -2(o_y - f_y b) & -2o_y & -2f_y b & 2f_y a & 2o_y a & 2(f_y + o_y b) \\ -2 & -2 & 0 & 0 & 2a & 2b \\ 0 & 0 & 0 & 0 & 0 & 0 \\ 0 & 0 & 0 & 0 & 0 & 0 \\ 0 & 0 & 0 & 0 & 0 & 0 \end{bmatrix}$$

$$\Pi_1 = \begin{bmatrix} -\epsilon_x & 0 & 0 & 0 & 0 & 0 \\ 0 & -\epsilon_y & 0 & 0 & 0 & 0 \\ 0 & 0 & -\epsilon_z & 0 & 0 & 0 \\ -\epsilon_y & 0 & 0 & 0 & 0 & 0 \\ -\epsilon_z & 0 & 0 & 0 & 0 & 0 \\ 0 & -\epsilon_z & 0 & 0 & 0 & 0 \end{bmatrix} \quad \Pi_2 = I_{6\times 6}$$

Recalling the *quaternion*, η is the scalar part, whose matrices dependencies will be handled at a later stage. In addition to that, at the image formation process $\{f_x, f_y, f_\theta, o_x, o_y\}$ are the intrinsic parameters of the camera and $\{a, b\}$ are the desired feature coordinates.

If the moment of inertia in J is equal for the three axis, i.e. $j_x = j_y = j_z$, then the bottom-right terms of A_2 are cancelled and the model dynamics do not depend on the interactions between the speed rotation in each axis, since the ω cross-product no longer appears.

3.3 2D Dynamic Models

Considering the problem of setting one feature to a specified position on the projected image by acting on the camera orientation through an input torque, as it is demonstrated in chapter 4 a 2-dimensional dynamic model provides enough information of the system dynamics to achieve this objective and stabilize the system.

This is somehow intuitive if one thinks that by rotating the camera only around the X and Y axes ("looking" up/down and to the left/right), it is possible to make the camera point at any direction. Eliminating the third degree of freedom forces the camera to maintain a constant angle around the Z axis.

Therefore, having also in mind that the 2D model is considerably less complex (see the following equations) than the 3D model, it is useful to develop the control synthesis and optimization based on it.

This simplification is done by making the following assumptions: $\epsilon_z = 0$, $\omega_z = 0$ and $\tau_z = 0$. Then, the model equations are refactored and redimensioned to eliminate the null terms. The resulting Quasi-LPV and DAR 2D models follow.

3.3.1 Quasi-LPV 2D Model

To define the Quasi-LPV 2D model, the system states and inputs are described as follows:

$$x = \begin{bmatrix} \epsilon_x \\ \epsilon_y \\ \omega_x \\ \omega_y \end{bmatrix} \quad \tau = \begin{bmatrix} \tau_x \\ \tau_y \end{bmatrix} \tag{40}$$

Being the resulting matrices for two dimensions are expressed by:

$$A = \begin{bmatrix} & \frac{1}{2}\eta & 0 \\ 0_{2x2} & 0 & \frac{1}{2}\eta \\ & 0_{2x2} & \end{bmatrix} \quad B = \begin{bmatrix} 0_{2x2} \\ j_x^{-1} & 0 \\ 0 & j_y^{-1} \end{bmatrix}$$

$$C = \begin{bmatrix} 2[f_\theta(\eta + a\epsilon_y - b\epsilon_x) - o_x(\epsilon_x + b\eta) + f_x b\epsilon_y] & -2[f_x(\eta + a\epsilon_y) - o_x(\epsilon_y - a\eta)] & 0 & 0 \\ 2[f_y(\eta + a\epsilon_y - b\epsilon_x) - o_y(\epsilon_x + b\eta)] & -2[o_y(\epsilon_y - a\eta)] & 0 & 0 \\ 0 & 0 & 1 & 0 \\ 0 & 0 & 0 & 1 \end{bmatrix} \tag{41}$$

Note that, as opposed to the 3D model, in this case none of the matrices for the rigid-body dynamics $A(\eta)$ and B are directly functions of the states, although $A(\eta)$ still depends on the quaternion through η. The output matrix $C(x, \eta)$, however, still has $\{\epsilon_x, \epsilon_y\}$ dependence.

3.3.2 DAR 2D Model

On the DAR 2D model, it is clear in (42) that not only the system has a lower order, but also the nonlinear vectors ξ and π.

$$x = \begin{bmatrix} \epsilon_x \\ \epsilon_y \\ \omega_x \\ \omega_y \end{bmatrix} \quad \xi = \begin{bmatrix} \epsilon_x\omega_y \\ \epsilon_y\omega_x \\ \omega_x\omega_y \end{bmatrix} \quad \pi = \begin{bmatrix} \epsilon_x^2 \\ \epsilon_y^2 \\ \epsilon_x\epsilon_y \end{bmatrix} \quad \tau = \begin{bmatrix} \tau_x \\ \tau_y \end{bmatrix} \tag{42}$$

The resulting matrices for two dimensions are then expressed by:

$$A_1 = \begin{bmatrix} 0_{2x2} & \begin{matrix} \frac{1}{2}\eta & 0 \\ 0 & \frac{1}{2}\eta \end{matrix} \\ 0_{2x2} & 0_{2x2} \end{bmatrix} \quad A_2 = 0_{4x3} \quad B_1 = \begin{bmatrix} 0_{2x2} \\ \begin{matrix} j_x^{-1} & 0 \\ 0 & j_y^{-1} \end{matrix} \end{bmatrix}$$

$$\Omega_1 = \begin{bmatrix} -\omega_y & 0 & 0 & 0 \\ 0 & -\omega_x & 0 & 0 \\ 0 & 0 & -\omega_y & 0 \end{bmatrix} \quad \Omega_2 = I_{3\times 3}$$

$$C_1 = \begin{bmatrix} 2(f_\theta\eta - o_x b\eta) & 2(o_x a\eta - f_x\eta) & 0 & 0 \\ 2(f_y\eta - o_y b\eta) & 2o_y a\eta & 0 & 0 \\ 0 & 0 & 1 & 0 \\ 0 & 0 & 0 & 1 \end{bmatrix} \quad C_2 = \begin{bmatrix} -2(o_x - f_\theta b) & -2(o_x - f_x a) & 2(f_\theta a + f_x b) \\ -2(o_y - f_y b) & -2o_y & 2f_y a \\ 0 & 0 & 0 \\ 0 & 0 & 0 \end{bmatrix}$$

$$\Pi_1 = \begin{bmatrix} -\epsilon_x & 0 & 0 & 0 \\ 0 & -\epsilon_y & 0 & 0 \\ -\epsilon_y & 0 & 0 & 0 \end{bmatrix} \quad \Pi_2 = I_{3\times 3}$$

(43)

Similarly to what happens in the Quasi-LPV 2D model, the nonlinear part of the rigid-body dynamics vanishes on the DAR since A_2 equals zero. The output, however, still has the nonlinear vector π as a system parameter.

4 CONTROL

4.1 Problem Definition

The control design problem, which is hereafter turned into an optimization problem, will be solved for both model representations considered in this work: *Quasi-LPV* and *DAR*.

In view of system (23), with states representing the camera rotation angle in terms of *quaternions* (ϵ) and rotation speed ω; and outputs (31) representing the error between a *feature* projection and its desired coordinates on the image and the rotation speed ω:

Problem 4.1. *Considering a closed-loop system defined by the set of nonlinear equations* (32) *for Quasi-LPV or* (36) *for DAR, determine a static output feedback control law that maximizes the estimate of the region of attraction inside a specified domain of interest in which the origin is guaranteed to be asymptotically stable.*

Note that two problems are actually embedded in Problem 4.1, one for Quasi-LPV system representation and one for DAR. It was kept as a single problem considering their similarity and for comparison of results between them.

4.2 Control Structure

After the determination of the models' matrices that represent the nonlinear system, in order to solve Problem 4.1, the feedback of the system is defined as:

$$\tau = Ky = K \begin{bmatrix} e \\ \omega \end{bmatrix} \tag{44}$$

where $K \in \mathbb{R}^{m \times p}$, being m the number of inputs and p the number of outputs of the system.

4.3 Stability Analysis

As stated in section 3.3, since this work deals with a one *feature* problem, the 2D model will be used and rotation around the Z camera axis won't be treated, being the parameters related to this additional degree of freedom assumed to be fixed as zero.

Considering this, adapting Theorem 4.1 from (KHALIL, 2002):

Lemma 4.1. *Let $x = 0$ be an equilibrium point for $\dot{x} = f(x)$. Given a domain of interest $x \in \mathcal{X}$ containing the origin, if there is a Lyapunov candidate function $V(x) = x^\intercal P x$ such that*

$$V(0) = 0,\ V(x) > 0 \quad \forall\, x \in \mathcal{X} - \{0\} \tag{45}$$

$$\dot{V}(x) = x^\intercal P \dot{x} + \dot{x}^\intercal P x < 0 \quad \forall\, x \in \mathcal{X} - \{0\} \tag{46}$$

$$\mathcal{R} = \{x : V(x) \leqslant 1\} \subset \mathcal{X} \tag{47}$$

Then $x = 0$ is an asymptotically stable equilibrium point and $\mathcal{R}$ is an estimate of the region of attraction, since every initial condition inside $\mathcal{R}$ asymptotically approaches the origin.

Based on that, the following topics are now addressed to analyze local asymptotic stability for equilibrium points, considering the requirements on region of attraction estimate: domain of interest, time-varying parameters and parameters based on the desired scenarios covered.

4.3.1 Domain of Interest

Let $x_\epsilon \coloneqq \epsilon$ and $x_\omega \coloneqq \omega$ represent the state vectors for the quaternion and the rotation speed, respectively (*e.g.* for a 2D system, $x_\epsilon = [x_{\epsilon 1} \quad x_{\epsilon 2}] = [x_1 \quad x_2]^\intercal$ and $x_\omega = [x_{\omega 1} \quad x_{\omega 2}] = [x_3 \quad x_4]^\intercal$). $\mathcal{X}$ can then be defined as the domain of interest, in which any control law designed for the system (23) will be valid, according to:

$$\mathcal{X} = \left\{ x_\epsilon \in \mathbb{R}^{n/2}, x_\omega \in \mathbb{R}^{n/2} : \sum_i \frac{x_{\epsilon i}^2}{\alpha_i} + \sum_i \frac{x_{\omega i}^2}{\beta_i} \leq 1 \right\},\ i = 1, \ldots, {}^n\!/_2 \tag{48}$$

where n is the number of states (system order) and $\mathcal{X}$ forms a hyperellipsoid, *i.e.*, a higher dimensional ellipsoid, with α_i being the squared length limit for the i^{th} dimension of ϵ and β_i being the squared length limit for the i^{th} dimension of ω.

This is done to assign an elliptic range for both ϵ and ω in which it is desired that the system respects the required stability characteristics. It is important to notice that this region of attraction estimate in ϵ can be projected on the screen according to (9) (with μ_0 taken as the center of the display, *i.e.*, $[0 \ \ 0 \ \ 1]^\intercal$).

The objective, therefore, is to design a control law that maximizes $\mathcal{R} \subset \mathcal{X}$ in which the origin is asymptotically stable. Then, it follows that:

$$\left\{ x_\epsilon^\intercal M^{-1} x_\epsilon + x_\omega^\intercal N^{-1} x_\omega \leq 1 \right\}, \ \forall x: \ x^\intercal P x \leq 1, \ i = 1, \ldots, {}^{n}/_{2} \tag{49}$$

where:

$$M^{-1} = \begin{bmatrix} \alpha_1^{-1} & 0 \\ 0 & \ddots \\ & \alpha_i^{-1} \end{bmatrix} \qquad N^{-1} = \begin{bmatrix} \beta_1^{-1} & 0 \\ 0 & \ddots \\ & \beta_i^{-1} \end{bmatrix} \tag{50}$$

By taking these relations and applying Lemma 2.2 ($\mathcal{S}$-procedure), equation (49) becomes equivalent to:

$$\exists \kappa \in \mathbb{R}^+ : \left\{ \kappa P - \begin{bmatrix} M^{-1} & 0 \\ 0 & N^{-1} \end{bmatrix} \succeq 0 \right\} \tag{51}$$

which defining $\kappa = 1$ (considering $\mathcal{R}$ is restricted to the edges of $\mathcal{X}$) and using Lemma 2.1 (Schur complement) can be stated as the following inequality (representing a restriction to the optimization problem):

$$\begin{bmatrix} P & I_n \\ I_n & \Upsilon \end{bmatrix} \succeq 0 \tag{52}$$

where $\Upsilon = \begin{bmatrix} M & 0 \\ 0 & N \end{bmatrix}$.

The following steps are part of the procedure to define α_i and β_i limits. While β_i is specified in step (c), α_i determination is complemented in next section, according to the polytope defined for the states which encloses the region $\mathcal{X}$.

(a) A desired angular range $\{\pm\psi_{\hat{X}}, \pm\psi_{\hat{Y}}\}$ inside or not of the camera field of view, but limited to $(-90°, 90°)$, is selected for $\hat{X}$ and $\hat{Y}$ axes of the display as a domain of interest.

(b) Considering the elliptic form of the domain of interest, the rotation limits around each camera axis are taken independently, resulting in:

$$q_{\psi_{\hat{X}}} = \begin{bmatrix} \cos(\frac{\psi_{\hat{X}}}{2}) \\ 0 \\ \sin(\frac{\psi_{\hat{X}}}{2}) \\ 0 \end{bmatrix} \quad q_{\psi_{\hat{Y}}} = \begin{bmatrix} \cos(\frac{\psi_{\hat{Y}}}{2}) \\ \sin(\frac{\psi_{\hat{Y}}}{2}) \\ 0 \\ 0 \end{bmatrix}$$
$$q_{lim} = \begin{bmatrix} \min\{\eta_{\psi_{\hat{X}}}, \eta_{\psi_{\hat{Y}}}\} & 1 \\ -\epsilon_{\psi_{\hat{Y}}} & \epsilon_{\psi_{\hat{Y}}} \\ -\epsilon_{\psi_{\hat{X}}} & \epsilon_{\psi_{\hat{X}}} \\ 0 & 0 \end{bmatrix} \tag{53}$$

where $\psi_{\hat{X}}$ is associated with a rotation around the camera Y axis and $\psi_{\hat{Y}}$ with a rotation around the camera X axis.

q_{lim} definition makes η limited to positive values, avoiding any discontinuities in $\eta = 0$ as already mentioned, and since the solution dynamics are continuous, if the initial condition has $\eta > 0$, it will always be positive. The value of ϵ, instead, is limited to $(-1, 1)$.

(c) The limits for ω depend on the $\{\pm\psi_{\hat{X}}, \pm\psi_{\hat{Y}}\}$ range specified, taking into account an estimation of the settling time. In this case, by setting an arbitrarily low settling time, the limits for ω represent a relaxed restriction. Considering that:

$$N = \begin{bmatrix} \beta_1 & 0 \\ 0 & \beta_2 \end{bmatrix} = \begin{bmatrix} \psi_{\hat{Y}}/t_s & 0 \\ 0 & \psi_{\hat{X}}/t_s \end{bmatrix} \tag{54}$$

where $t_s[s]$ is an approximate maximum desired settling time.

Alternatively, as mentioned previously, if no restriction is to be imposed to ω, (49) can be written as

$$\left\{ x_\epsilon^\intercal M^{-1} x_\epsilon \leq 1 \right\},\ \forall x:\ x_\epsilon^\intercal P_\epsilon x_\epsilon \leq 1,\ i = 1, \ldots, n/2, \tag{55}$$

where $P = \begin{bmatrix} P_\epsilon & P_{12} \\ P_{12}^\intercal & P_\omega \end{bmatrix}$, resulting in inequality

$$\begin{bmatrix} P_\epsilon & I_{n/2} \\ I_{n/2} & M \end{bmatrix} \succeq 0 \tag{56}$$

However, as discussed in (SALTON *et al.*, 2017), not restricting ω to a defined domain of interest can result in additional conservativeness and a smaller region of attraction estimate for ϵ, since the stability conditions would have to be satisfied for the whole possible range of ω.

4.3.2 Polytopic Approach for Time-Varying Parameters and Uncertainties

In a similar approach to (TROFINO; DEZUO, 2014; SALTON *et al.*, 2017; SARAIVA, 2019), polytopes to evaluate the system for stability will be defined for both the time-varying parameters and for other parameters that are expected to have a predefined range, which are part of the state matrices. The difference here is that the domain of interest $\mathcal{X}$ in which to maximize the actual region of interest $\mathcal{R}$ is not a polytope itself, but norm-based.

Therefore, in order to have a finite set of equations ensuring stability of the domain of interest by evaluating points that are representative for this purpose, a convex hull of vertices containing the ellipsoid is defined so that $\mathcal{X} \subset \bar{\mathcal{X}} \subset \mathcal{V}_{\bar{\mathcal{X}}}$, where $\bar{\mathcal{X}}$ is the domain specified in (57) which is contained by $\mathcal{V}_{\bar{\mathcal{X}}}$. Note that, to have a less conservative set of

vertices (closer to the actual norm-based domain of interest $\mathcal{X}$), it was chosen to have an 8-sided polytope, *i.e.*, an octagon for the limits of ϵ.

Then, based on q_{lim}:

$$\bar{\mathcal{X}} = \left\{ x \in \mathbb{R}^n : |x_1| \leq \epsilon_{\psi_{\hat{Y}}} \cos\phi_i,\ |x_2| \leq \epsilon_{\psi_{\hat{X}}} \sin\phi_i \right\},\ i = 1, \ldots, 8 \tag{57}$$

where $\epsilon_{\psi_{\hat{X}}}, \epsilon_{\psi_{\hat{Y}}}$ are obtained from (53), $\phi_1, \ldots, \phi_8$ are equally spaced angles from 0 to 2π rad and $\bar{\mathcal{X}} \subset \mathcal{V}_{\bar{\mathcal{X}}}$.

With the definition of this polytope, which will be used to assess the stability of the system, and completing the definition of the parameters for the domain of interest: as stated previously, $\mathcal{X} \subset \mathcal{V}_{\bar{\mathcal{X}}}$. For that to be true, and to delimit correctly this ellipsoid region for ϵ (*i.e.*, tangent to $\bar{\mathcal{X}} \subset \mathcal{V}_{\bar{\mathcal{X}}}$), it is maximized as follows, with a procedure adapted from (POLCZ; SZEDERKÉNYI; PÉNI, 2015):

First, new vertices $\mathcal{V}_{\mathcal{Z}}$ are defined as the average points of $\mathcal{V}_{\bar{\mathcal{X}}}$, therefore resulting in a new (inner) polytope $\mathcal{Z} \in \mathcal{V}_{\mathcal{Z}}$:

$$\mathcal{Z} = \left\{ z \in \mathbb{R}^n : \begin{array}{l} z_1 \leq \epsilon_{\psi_{\hat{Y}}} \frac{\cos\phi_i + \cos\phi_{i+1}}{2},\ z_2 \leq \epsilon_{\psi_{\hat{X}}} \frac{\sin\phi_i + \sin\phi_{i+1}}{2},\ i = 1, \ldots, 7 \\ z_1 \leq \epsilon_{\psi_{\hat{Y}}} \frac{\cos\phi_i + \cos\phi_1}{2},\ z_2 \leq \epsilon_{\psi_{\hat{X}}} \frac{\sin\phi_i + \sin\phi_1}{2},\ i = 8 \end{array} \right\} \tag{58}$$

where $z = \begin{bmatrix} z_1 & z_2 \end{bmatrix}^\intercal$.

The inner polytope definition has the objective of preventing the domain of interest for RoA estimate from exceeding the limits of the outer polytope. For that, the domain of interest $\mathcal{X}$ is maximized within the limits of $\mathcal{Z}$ by finding:

OP1:

$$\max_{M,\upsilon} \upsilon : \begin{cases} M \succeq 0,\ \upsilon \geq 1 \\ \begin{bmatrix} z \\ 1 \end{bmatrix}^\intercal \begin{bmatrix} M & 0 \\ 0 & -\upsilon \end{bmatrix} \begin{bmatrix} z \\ 1 \end{bmatrix} \geq 0,\ \begin{bmatrix} z \\ 1 \end{bmatrix}^\intercal \begin{bmatrix} M & 0 \\ 0 & -1 \end{bmatrix} \begin{bmatrix} z \\ 1 \end{bmatrix} \leq 0 \end{cases} \tag{59}$$

where $M = \begin{bmatrix} \alpha_1 & 0 \\ 0 & \alpha_2 \end{bmatrix}$ is the matrix to be used in (52).

The computation of the domain of interest for ϵ is illustrated in figure 3.

To achieve a solution that successfully meets the objectives considering the desired scope and existing constraints, the range of parameters that are expected to vary not only in real-time, but also for the all anticipated scenarios when the solution is applied to the actual system or model, has to be taken into account, otherwise the solution won't be satisfactory within the whole range, degrading any necessary robustness.

Hence, one of the available methods that can be employed to address such requirements is to map the expected range of the varying parameters and include them as uncertainties, resulting therefore in an uncertain system. This approach, considering more

Figure 3 – Forming the domain of interest.

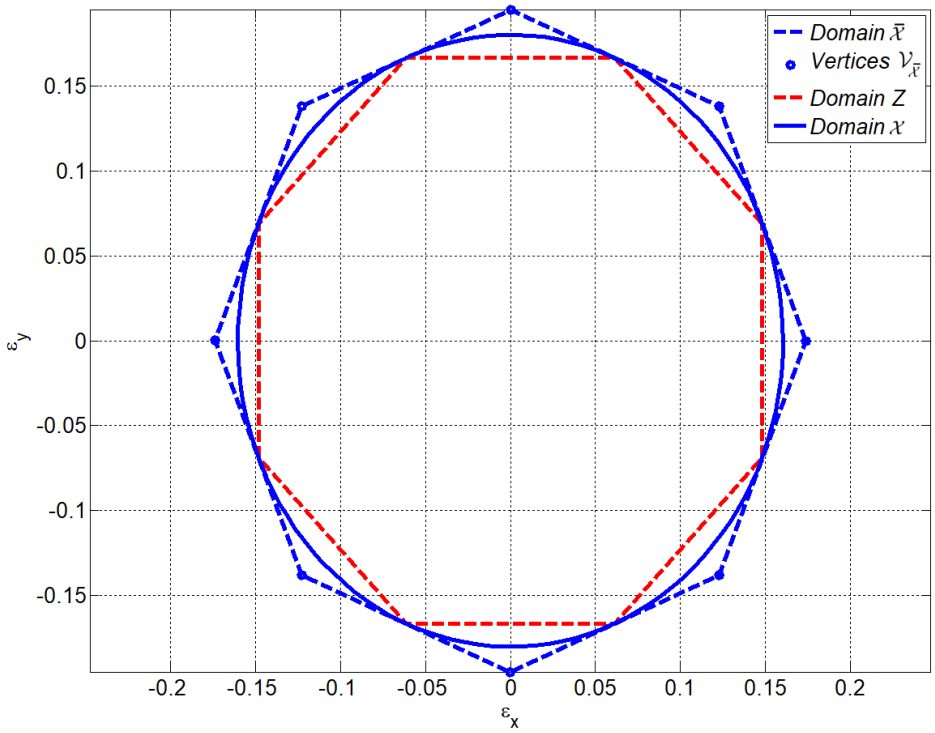

Source: from the author

specifically uncertain rational nonlinear systems, is thoroughly studied in (TROFINO; DEZUO, 2014), being conveniently used, for example, in (SALTON *et al.*, 2017) and (SARAIVA, 2019).

In the present work, in addition to the parameters (x, η) that are taken as arguments of the model representations in (32) and (36) (since they are inherently variables of the functions), the desired position of the feature in the image projection, represented by $\{a, b\}$ in (26), is also assigned a range so it is possible to define where the feature is intended to be projected inside that range.

With that in view, these additional parameters are defined as follows, forming a new polytope, $\Delta \subset \mathcal{V}_\Delta$:

$$\Delta = \left\{ \begin{array}{l} \delta_1 \coloneqq \eta : \min\left\{\eta_{\psi_{\hat{X}}}, \eta_{\psi_{\hat{Y}}}\right\} \leq \delta_1 \leq 1 \\ \delta_2 \coloneqq a : |\delta_2| \leq \tan\psi_{\hat{Y}} \\ \delta_3 \coloneqq b : |\delta_3| \leq \tan\psi_{\hat{X}} \\ \delta_4 \coloneqq a\eta : \underline{\delta_4} \leq \delta_4 \leq \bar{\delta_4} \\ \delta_5 \coloneqq b\eta : \underline{\delta_5} \leq \delta_5 \leq \bar{\delta_5} \end{array} \right\}, \delta_i \in \mathbb{R}, i = 1, \ldots, 5 \qquad (60)$$

where $\delta = \begin{bmatrix} \delta_1 & \delta_2 & \delta_3 & \delta_4 & \delta_5 \end{bmatrix}^\intercal$, $\eta_{\psi_{\hat{X}}}, \eta_{\psi_{\hat{Y}}}$ are defined in (53), $\psi_{\hat{X}}, \psi_{\hat{Y}}$ are defined in section 4.3.1 item (a), $[\underline{\delta_4}, \bar{\delta_4}]$ are the minimum and maximum values of all combinations of $\delta_2\delta_1$, respectively, and $[\underline{\delta_5}, \bar{\delta_5}]$ are the minimum and maximum values of all combinations of $\delta_3\delta_1$, respectively.

Considering the uncertainties δ_2 and δ_3 are associated with the normalized desired feature coordinates $\{a, b, 1\}$, defining the limits of $|\delta_2|$ to $\tan\psi_{\hat{X}}$ actually means that the coordinate a values are limited by that angle. This is established by the relation $\tan\psi_{\hat{X}} \pm \frac{a}{1}$ (feature's first over third coordinate). The same happens for the coordinate b and $\psi_{\hat{Y}}$, related to δ_3 definition.

Completing the set of parameters inside the state matrices, some of them are, however, considered constant and therefore given prior to the analysis and not defined as uncertainties, being them: camera intrinsic parameters $\{o_x, o_y, f_x, f_y, f_\theta\}$ and camera inertia parameters $\{j_x, j_y, j_z\}$.

4.3.3 Remarks on Stability Analysis

As stated in the previous sections, to assess the closed-loop system in all the necessary vertices and guarantee asymptotic stability in the estimate of the region of attraction with the control design proposed, there has to be a matrix inequality for each of the combinations of parameters composing the vertices of the polytopes, and also for the combination of these polytopes.

Then, considering the polytopes $\bar{\mathcal{X}} \subset \mathcal{V}_{\bar{\mathcal{X}}}$ in (57) and $\Delta \subset \mathcal{V}_\Delta$ in (60), the matrices that define system (23) in its Quasi-LPV representation (41) and DAR (43) need to be evaluated at all the mentioned vertices. This makes the matrix inequalities which assess system stability to be dependent on $(x, \delta) \in \mathcal{V}_{\bar{\mathcal{X}}} \times \mathcal{V}_\Delta$ (TROFINO; DEZUO, 2014; SALTON *et al.*, 2017).

4.4 Control Design

Given the definition of the domain of interest and the polytopes evaluated, the following theorems, which are adapted from (COUTINHO *et al.*, 2004; SALTON *et al.*, 2017; SARAIVA, 2019), address the asymptotic stability of the closed-loop 2D camera system using the Quasi-LPV representation and DAR, respectively, and consequently solving Problem 4.1:

Theorem 1. (Quasi-LPV Stability) *Considering the Quasi-LPV representation* (32) *of system* (23) *and letting* (44) *be the static output feedback control law for the closed-loop system: Suppose there are matrices $K \in \mathbb{R}^{m\times n}$ and $Q = Q^\intercal \succeq 0 \in \mathbb{R}^{n\times n}$ such that for all (x, δ) evaluated at the convex set of vertices $\mathcal{V}_{\bar{\mathcal{X}}} \times \mathcal{V}_\Delta$ that contain the domain of interest $\mathcal{X}$ given by* (48) *and the polytopic region Δ given by* (60)*:*

$$\text{He}\{(A(x,\delta) + BKC(x,\delta))Q\} \prec 0 \tag{61}$$

$$\begin{bmatrix} Q & Q \\ Q & \Upsilon \end{bmatrix} \succeq 0 \tag{62}$$

Then, the origin is an asymptotically stable equilibrium point for all trajectories starting in:

$$\mathcal{R} = \{x \in \mathbb{R}^n : x^\intercal P x \leq 1\} \subset \mathcal{X} \tag{63}$$

where $P = Q^{-1}$.

Proof: Considering a Lyapunov candidate function $V(x) = x^\intercal P x$, with $P = Q^{-1}$, the assumption taken that Q is a symmetric positive matrix leads to the conclusion that the function is positive definite. Then, in order to verify that (61) implies $\dot{V}(x) < 0$, by recalling the Quasi-LPV model equation (32) and including on it the control law $\tau = Ky$, the dynamic of x can be set as (dependence on (x, δ) is omitted from the proof):

$$\dot{x} = Ax + BKCx \tag{64}$$

And, taking the derivative of $V(x)$ as in (46), it can be shown that:

$$\dot{V}(x) = x^\intercal PAx + x^\intercal PBKCx + x^\intercal A^\intercal Px + x^\intercal C^\intercal K^\intercal B^\intercal Px \tag{65}$$

so that the asymptotic stability can be guaranteed if $\text{He}\{PA + PBKC\} \prec 0$, which by pre and post-multiplying by Q is equivalent to (61).

Regarding the region of attraction estimate for the system, one can show that it will be constrained to the elliptic range defined by $\mathcal{X}$, as stated in (63), if it is proven that (62) implies (49). For that, the process described in this section leading from the definition of the domain of interest in (48) to the inequality (52) is recalled. Considering that, it suffices to take Lemma 2.1 (Schur complement) and show that (62) can be written as:

$$Q - Q\Upsilon^{-1}Q \succeq 0 \tag{66}$$

which by pre and post-multiplying by P and applying again the Schur complement is equivalent to (52).

Completing the proof, if BMIs (61) and (62) are satisfied for all vertices $\mathcal{V}_{\bar{\mathcal{X}}} \times \mathcal{V}_\Delta$, by convexity it can be assumed that it is true $\forall x \in \mathcal{X},\ \forall \delta \in \Delta$ and consequently $\forall x \in \mathcal{R}$.

Theorem 2. (DAR Stability) *Considering the DAR representation* (36) *of system* (23) *and letting* (44) *be the static output feedback control law for the closed-loop system: Suppose there are matrices* $K \in \mathbb{R}^{m \times n}$, $Q = Q^\intercal \succeq 0 \in \mathbb{R}^{n \times n}$, $W_1 \in \mathbb{R}^{n_\xi \times n_\xi}$ *and* $W_2 \in \mathbb{R}^{n_\pi \times n_\pi}$ *such that for all* (x, δ) *evaluated at the convex set of vertices* $\mathcal{V}_{\bar{\mathcal{X}}} \times \mathcal{V}_\Delta$ *that contain the domain of interest* $\mathcal{X}$ *given by* (48) *and the polytopic region* Δ *given by* (60)*:*

$$\begin{bmatrix} \text{He}\{(A_1(\delta) + B_1KC_1(\delta))Q\} & A_2(\delta)W_1^\intercal + Q\Omega_1^\intercal(x) & (B_1KC_2(\delta))W_2^\intercal + Q\Pi_1^\intercal(x) \\ & \text{He}\{\Omega_2 W_1^\intercal\} & 0 \\ \star & & \text{He}\{\Pi_2 W_2^\intercal\} \end{bmatrix} \prec 0 \tag{67}$$

$$\begin{bmatrix} Q & Q \\ Q & \Upsilon \end{bmatrix} \succeq 0 \tag{68}$$

Then, the origin is an asymptotically stable equilibrium point for all trajectories starting in:

$$\mathcal{R} = \{x \in \mathbb{R}^n : x^\intercal P x \leq 1\} \subset \mathcal{X} \tag{69}$$

where $P = Q^{-1}$.

Proof: Considering a Lyapunov candidate function $V(x) = x^\intercal P x$, with $P = Q^{-1}$, the assumption taken that Q is a symmetric positive matrix leads to the conclusion that the function is positive definite. Then, in order to verify that (67) implies $\dot{V}(x) < 0$, first the dynamic of x is recalled from the DAR model in (36) taking into account the control law $\tau = Ky$, so that (dependence on (x, δ) is omitted from the proof):

$$\dot{x} = A_1 x + A_2 \xi + B_1 K C_1 x + B_1 K C_2 \pi \tag{70}$$

The derivative of $V(x)$ then becomes for the DAR:

$$\dot{V}(x) = \text{He}\{x^\intercal P A_1 x + x^\intercal P B_1 K C_1 x + x^\intercal P A_2 \xi + x^\intercal P B_1 K C_2 \pi\} \tag{71}$$

By defining a vector $\zeta = \begin{bmatrix} x^\intercal & \xi^\intercal & \pi^\intercal \end{bmatrix}^\intercal$, in a similar manner as (SALTON *et al.*, 2017), it is possible to convert (46) it into the matrix inequality that follows:

$$\zeta^\intercal \begin{bmatrix} \text{He}\{PA_1 + PB_1 K C_1\} & PA_2 & PB_1 K C_2 \\ A_2^\intercal P & 0 & 0 \\ C_2^\intercal K^\intercal B_1^\intercal P & 0 & 0 \end{bmatrix} \zeta < 0 \tag{72}$$

After that, the algebraic equations of the DAR are introduced in the stability problem together with some scaling variables, aiming to guarantee feasibility of the solution (TROFINO; DEZUO, 2014). To achieve this, Lemma 2.3 (Finsler's Lemma) is applied thus obtaining the following matrix inequality, equivalent to $\dot{V}(x) < 0$ considering $[\Omega_1 \;\; \Omega_2 \;\; 0]\,\zeta = 0$ and $[\Pi_1 \;\; 0 \;\; \Pi_2]\,\zeta = 0$ according to the model representation defined in (36):

$$\dot{V}(x) + \text{He}\left\{\xi L_1 \begin{bmatrix} \Omega_1 & \Omega_2 & 0 \end{bmatrix} \zeta\right\} + \text{He}\left\{\pi L_2 \begin{bmatrix} \Pi_1 & 0 & \Pi_2 \end{bmatrix} \zeta\right\} < 0 \tag{73}$$

which similarly to (72) turns into the following matrix form:

$$\begin{bmatrix} \text{He}\{PA_1 + PB_1 K C_1\} & PA_2 + \Omega_1^\intercal L_1^\intercal & PB_1 K C_2 + \Pi_1^\intercal L_2^\intercal \\ A_2^\intercal P + L_1 \Omega_1 & \text{He}\{L_1 \Omega_2\} & 0 \\ C_2^\intercal K^\intercal B_1^\intercal P + L_2 \Pi_1 & 0 & \text{He}\{L_2 \Pi_2\} \end{bmatrix} < 0 \tag{74}$$

By pre and post-multiplying (74) by $diag(Q, W_1, W_2)$ and its transpose, respectively, where $W_1 = L_1^{-1}$ and $W_2 = L_2^{-1}$, it finally results in (67).

The region of attraction estimate for the system, once again, can be shown to be constrained to the elliptic range defined by $\mathcal{X}$, as stated in (69), in case (68) implies (49). The process described in this section leading from the definition of the domain of interest in (48) to the inequality (52) is used and therefore it suffices to take Lemma 2.1 (Schur complement) and show that (68) can be written as:

$$Q - Q\Upsilon^{-1}Q \succeq 0 \tag{75}$$

which by pre and post-multiplying by P and applying again the Schur complement is equivalent to (52).

Therefore, if BMIs (67) and (68) are satisfied for all vertices $\mathcal{V}_{\bar{\mathcal{X}}} \times \mathcal{V}_{\Delta}$, by convexity it can be assumed that it is true $\forall x \in \mathcal{X},\ \forall \delta \in \Delta$ and consequently $\forall x \in \mathcal{R}$.

4.5 Optimization Method

Problem 4.1 brings up the necessity of maximizing the estimate of the region of attraction of the solution, inside a pre-specified domain. From that, it is a natural way forward to think of it as an optimization problem with restrictions.

First, it is important to mention that the matrix inequalities conditions obtained in section 4.3 for asymptotic stability can be classified as BMIs, which, as already explained in section 2.3, have NP-hard feasibility analysis (TOKER; OZBAY, 1995). Therefore, the solution strategy developed in this work includes finding a way to linearize the optimization problems (*i.e.*, transforming the BMIs into LMIs) before applying the optimization process.

Several methods exist for this purpose, as described in section 1.1, being the P-K iteration algorithm used to solve the problems handled herein. This method was proposed by (EL GHAOUI; BALAKRISHNAN, 1994) (referred to as V-K), while (SADABADI; PEAUCELLE, 2016) explains it in the context of the available methods for BMI optimization solution, providing a review of the static output feedback design methods that achieve a set of LMIs to be solved, mostly iterative ones.

Some of these iterative approaches are able to convert a non-convex SOF design into a convex optimization problem (SADABADI; PEAUCELLE, 2016). More specifically, having in mind for example the LMI in (61) (which results from the dual formulation of the Lyapunov equation), the P-K algorithm makes it convex in Q for a fixed K, in an attempt to achieve a feasible solution used to find $P = Q^{-1}$, and convex in K for a fixed Q, making it possible to even impose a structured gain if necessary (SADABADI; PEAUCELLE, 2016).

As mentioned in (EL GHAOUI; BALAKRISHNAN, 1994), this is an heuristic algorithm and does not guarantee global stability. However, even though it is a local optimization procedure, it can achieve good results depending on its initialization. Also as an

advantage of the P-K method, if a step of the iteration is infeasible, it does not directly imply that a feasible controller is non-existent (EL GHAOUI; BALAKRISHNAN, 1994), meaning that if it continues running efficiently for each step's LMIs it is possible that convergence is achieved.

To solve the SOF problem for the nonlinear camera system, synthesized by (61)-(62) for the the Quasi-LPV representation and (67)-(68) for the DAR model, considering the objective is to maximize the region of attraction estimate (restricted to a domain of interest) to which the system is asymptotically stable, the minimization objective function initially envisioned for the P-K algorithm is slightly modified. Instead of aiming at minimizing the largest eigenvalue of the matrix involved in the LMI by using an auxiliary scalar variable until it becomes negative, achieving stability (SADABADI; PEAUCELLE, 2016; EL GHAOUI; BALAKRISHNAN, 1994), the objectives for each iteration step are set as follows:

- For a fixed K: the trace of P (inverse of Q) will be minimized to achieve a larger region of attraction estimate (the exact objective function will be explained in the next sections);
- For a fixed P (through a fixed Q): the absolute value of the trace of the resulting matrix on the left side of equations (61) or (67) is minimized. This is done to maximize $\dot{V}(x)$ such that the system is still asymptotically stable (according to the restrictions), considering in the following step this will help approximating the estimate of the region of attraction to its stability limits *i.e.*, being further enlarged.

4.5.1 Algorithm Initialization

In order to improve the quality of the important initialization of the P-K algorithm, an initial value for the gain K is obtained through the following process:

A linearized model of the system is evaluated at the equilibrium point at the center of the image, with desired position at the same position, *i.e.*, with:

$$q_{eq} = \begin{bmatrix} 1 \\ 0 \\ 0 \\ 0 \end{bmatrix} \qquad \omega_{eq} = \begin{bmatrix} 0 \\ 0 \\ 0 \end{bmatrix} \qquad \bar{\mu}_{eq} = \begin{bmatrix} 0 \\ 0 \\ 1 \end{bmatrix} \tag{76}$$

From that, it is possible to estimate a gain matrix that stabilizes the system at the referred point. Considering that it is likely that the system behavior will be similar if evaluated at a point very close to the origin (infinitesimal distance), by having this initial estimate of K and applying it to the first step of the optimization, the algorithm will be able to look for a region of attraction estimate larger than this point in which the system is still asymptotically stable.

The linearized state matrices become

$$A = \begin{bmatrix} 0_{2x2} & \begin{matrix} \frac{1}{2} & 0 \\ 0 & \frac{1}{2} \end{matrix} \\ 0_{2x2} & 0_{2x2} \end{bmatrix} \quad B = \begin{bmatrix} 0_{2x2} \\ \begin{matrix} j_x^{-1} & 0 \\ 0 & j_y^{-1} \end{matrix} \end{bmatrix}$$

$$C = \begin{bmatrix} 2f_\theta & -2f_x & 0 & 0 \\ 2f_y & 0 & 0 & 0 \\ 0 & 0 & 1 & 0 \\ 0 & 0 & 0 & 1 \end{bmatrix} \tag{77}$$

Then, by taking the LMI in (61), changing the state matrices $\{A, B, C\}$ by the linearized ones in (77) and substituting $Z \in \mathbb{R}^{m \times n} : Z = KCQ$, it suffices to solve the following optimization problem, adapted from (SALTON *et al.*, 2017):

OP2:

$$\min_{Q,\, Z,\, N} \text{trace}(N) : \begin{cases} AQ + QA^\intercal + BZ + Z^\intercal B^\intercal \prec 0 \\ \begin{bmatrix} Q & I \\ I & N \end{bmatrix} \succeq 0 \end{cases} \tag{78}$$

where $N = N^\intercal \in \mathbb{R}^{n \times n}$.

Using Lemma 2.1 (Schur complement), the bottom line of (78) implies $N \succeq Q^{-1} = P$, implicitly maximizing $\mathcal{R}$ since $\text{trace}(N) > \text{trace}(P)$.

Of course, at this stage there is no need to either define an LMI to restrict the DoI or make use of a polytopic approach for the stability conditions, since the system is linearized at a specified point.

Then, to acquire the initial estimated gain K, it follows that:

$$K_{init} = ZPC^{-1} \tag{79}$$

Note, from (77), that the linearized matrix C will always be invertible, since the intrinsic parameters f_x and f_y will never be zero, making it a nonsingular matrix.

4.5.2 Resulting Optimization Problems

As previously explained, since the P-K algorithm is initialized with a non-arbitrary pre-calculated gain, the first step is chosen as the one with fixed $K = K_{init}$.

Then, since each iteration is comprised of two steps, for each model being analyzed two optimization problems will be proposed. In addition to this, in the optimization problems involving the minimization of P, the same approach of OP2 will be taken by using the auxiliary decision variable N, so that the RoA estimate is maximized considering $\text{trace}(N) > \text{trace}(P)$.

Quasi-LPV Stability

OP3 (fixed K)**:**

$$\min_{Q,\,N} \text{trace}(N) : \begin{cases} (61),\ (62),\ \forall x \in \mathcal{V}_{\bar{\mathcal{X}}},\ \forall \delta \in \mathcal{V}_{\Delta} \\ \begin{bmatrix} Q & I \\ I & N \end{bmatrix} \succeq 0 \end{cases} \tag{80}$$

OP4 (fixed P)**:**

$$\min_{K,\,N} |\text{trace}(\Lambda)| : \begin{cases} (61),\ \forall x \in \mathcal{V}_{\bar{\mathcal{X}}},\ \forall \delta \in \mathcal{V}_{\Delta} \\ \begin{bmatrix} Q & I \\ I & N \end{bmatrix} \succeq 0 \end{cases} \tag{81}$$

where Λ is the resulting matrix on the left side of equation (61).

DAR Stability

OP5 (fixed K)**:**

$$\min_{Q,\,W_1,\,W_2,\,N} \text{trace}(N) : \begin{cases} (67),\ (68),\ \forall x \in \mathcal{V}_{\bar{\mathcal{X}}},\ \forall \delta \in \mathcal{V}_{\Delta} \\ \begin{bmatrix} Q & I \\ I & N \end{bmatrix} \succeq 0 \end{cases} \tag{82}$$

OP6 (fixed P)**:**

$$\min_{K,\,W_1,\,N} |\text{trace}(\Lambda)| : \begin{cases} (67),\ \forall x \in \mathcal{V}_{\bar{\mathcal{X}}},\ \forall \delta \in \mathcal{V}_{\Delta} \\ \begin{bmatrix} Q & I \\ I & N \end{bmatrix} \succeq 0 \end{cases} \tag{83}$$

where Λ is the resulting matrix on the left side of equation (67).

As it can be expected, the LMI for the DoI restriction is not present in the optimization problems with fixed P, since it involves only the $Q = P^{-1}$ variable.

4.6 Performance Extensions

4.6.1 Exponential Decay Rate

Considering the same system described for Problem 4.1:

Problem 4.2. *Determine a static output feedback control law that maximizes the estimate of the region of attraction, inside a specified domain of interest, in which every initial state approaches the origin asymptotically at a decay rate of at least σ.*

To address this performance problem, it is necessary to introduce the following definition, taken from (CASTRO *et al.*, 2020), that will serve as a basis to determine conditions

that guarantee the solution of the problem.

Definition 4.1. (σ-Exponential Convergence) *The trajectories $x(t)$ are said to converge exponentially to zero in $\mathcal{R}$ if there exist scalars $\varepsilon > 0$ and $\sigma > 0$ such that*

$$\|x(t)\| \leq \varepsilon \|x(0)\| e^{-\sigma t} \; \forall \; t \geq 0, \; \forall \; x(0) \in \mathcal{R} \subseteq \mathbb{R}^n \tag{84}$$

In this case, the trajectories $x(t)$ approach the origin with an exponential decay rate greater than σ.

Given the definition above, the domain of interest $\mathcal{X}$ in (48) and polytopes $\bar{\mathcal{X}}$ in (57) and Δ in (60), the following theorems, adapted from (CASTRO, 2019; SARAIVA, 2019; SALTON *et al.*, 2017) and using also concepts present in (BOYD *et al.*, 1994), address the asymptotic stability with exponential performance of the closed-loop 2D camera system.

Theorem 3. (Quasi-LPV Decay Rate) *Considering the Quasi-LPV representation* (32) *of system* (23) *and letting* (44) *be the static output feedback control law for the closed-loop system: Suppose there are matrices $K \in \mathbb{R}^{m \times n}$ and $Q = Q^{\intercal} \succeq 0 \in \mathbb{R}^{n \times n}$ and a positive scalar $\sigma \in \mathbb{R}$ such that for all (x, δ) evaluated at the convex set of vertices $\mathcal{V}_{\bar{\mathcal{X}}} \times \mathcal{V}_{\Delta}$:*

$$\text{He}\{(A(x,\delta) + BKC(x,\delta))Q + \sigma Q\} \prec 0 \tag{85}$$

$$\begin{bmatrix} Q & Q \\ Q & \Upsilon \end{bmatrix} \succeq 0 \tag{86}$$

Then, all closed-loop trajectories starting in $\mathcal{R}$ asymptotically approach the origin at a decay rate of at least σ, being this region of attraction estimate defined as:

$$\mathcal{R} = \{x \in \mathbb{R}^n : x^{\intercal} P x \leq 1\} \subset \mathcal{X} \tag{87}$$

where $P = Q^{-1}$.

Proof: Taking credit from the proof for Theorem 1, which demonstrates how the asymptotic stability criteria are transformed into a set of conditions based on matrix inequalities, it follows that, by adding the decay rate term in (65) and assessing the stability condition (46),

$$\text{He}\{PA + PBKC\} + 2\sigma P \prec 0, \tag{88}$$

which is equivalent to (85) by pre and post-multiplying by Q, and also to:

$$\dot{V}(x,\delta) < -2\sigma V(x) \tag{89}$$

The result of this differential inequality is, then:

$$V(x(t)) < V(x(0)) e^{-2\sigma t}, \forall x(0) \in \mathcal{R} \tag{90}$$

which, considering $\varepsilon = 1$ regarding Definition 4.1, completes the proof for the exponential decay rate problem with Quasi-LPV system representation. Note that, for polytopic systems, this supplementary restriction adds constraints to the eigenvalues of all combinations of $(A_i + B_i K C_i)$ matrices, $i = 1, \ldots, n_{\mathcal{V}_{\bar{\mathcal{X}}} \times \mathcal{V}_\Delta}$, which are assessed in each matrix inequality.

Theorem 4. (DAR Decay Rate) *Considering the DAR representation* (36) *of system* (23) *and letting* (44) *be the static output feedback control law for the closed-loop system: Suppose there are matrices $K \in \mathbb{R}^{m \times n}$, $Q = Q^\intercal \succeq 0 \in \mathbb{R}^{n \times n}$, $W_1 \in \mathbb{R}^{n_\xi \times n_\xi}$ and $W_2 \in \mathbb{R}^{n_\pi \times n_\pi}$ and a positive scalar $\sigma \in \mathbb{R}$ such that for all (x, δ) evaluated at the convex set of vertices $\mathcal{V}_{\bar{\mathcal{X}}} \times \mathcal{V}_\Delta$:*

$$\begin{bmatrix} \text{He}\{(A_1(\delta) + B_1 K C_1(\delta))Q + \sigma Q\} & A_2(\delta)W_1^\intercal + Q\Omega_1^\intercal(x) & (B_1 K C_2(\delta))W_2^\intercal + Q\Pi_1^\intercal(x) \\ \star & \text{He}\{\Omega_2 W_1^\intercal\} & 0 \\ & & \text{He}\{\Pi_2 W_2^\intercal\} \end{bmatrix} \prec 0 \tag{91}$$

$$\begin{bmatrix} Q & Q \\ Q & \Upsilon \end{bmatrix} \succeq 0 \tag{92}$$

Then, all closed-loop trajectories starting in $\mathcal{R}$ asymptotically approach the origin at a decay rate of at least σ, being this region of attraction estimate defined as:

$$\mathcal{R} = \{x \in \mathbb{R}^n : x^\intercal P x \leq 1\} \subset \mathcal{X} \tag{93}$$

where $P = Q^{-1}$.

Proof: Taking credit from the proof for Theorem 2, which demonstrates how the asymptotic stability criteria are transformed into a set of conditions based on matrix inequalities, it follows that, by adding the decay rate term in (74) and assessing the stability condition (46),

$$\begin{bmatrix} \text{He}\{PA_1 + PB_1 K C_1 + \sigma P\} & PA_2 + \Omega_1^\intercal L_1^\intercal & PB_1 K C_2 + \Pi_1^\intercal L_2^\intercal \\ A_2^\intercal P + L_1 \Omega_1 & \text{He}\{L_1 \Omega_2\} & 0 \\ C_2^\intercal K^\intercal B_1^\intercal P + L_2 \Pi_1 & 0 & \text{He}\{L_2 \Pi_2\} \end{bmatrix} < 0 \tag{94}$$

which is equivalent to (91) by pre and post-multiplying by $diag(Q, W_1, W_2)$ and its transpose, and also to:

$$\dot{V}(x) + 2\sigma V(x) + \text{He}\left\{\xi L_1 \begin{bmatrix} \Omega_1 & \Omega_2 & 0 \end{bmatrix} \zeta\right\} + \text{He}\left\{\pi L_2 \begin{bmatrix} \Pi_1 & 0 & \Pi_2 \end{bmatrix} \zeta\right\} < 0 \tag{95}$$

Since $[\Omega_1 \;\; \Omega_2 \;\; 0]\,\zeta = 0$ and $[\Pi_1 \;\; 0 \;\; \Pi_2]\,\zeta = 0$, (95) becomes:

$$\dot{V}(x, \delta) < -2\sigma V(x) \tag{96}$$

The result of this differential inequality is, then:

$$V(x(t)) < V(x(0))e^{-2\sigma t}, \forall x(0) \in \mathcal{R} \tag{97}$$

which, considering $\varepsilon = 1$ regarding Definition 4.1, completes the proof for the exponential decay rate problem with DAR system representation.

Considering the proposed Theorems 3 and 4, in a similar process as explained before in 4.5, they are turned into optimization problems to maximize the estimate of the region of attraction, in which the P-K iterative algorithm (EL GHAOUI; BALAKRISHNAN, 1994; SADABADI; PEAUCELLE, 2016) is used. For that, the same initial estimation for K is taken as in (79), based on the solution of (78).

With that, it is possible to define the following optimization problems with the objective of maximizing the region of attraction estimate considering Quasi-LPV and DAR representations, regarding Problem 4.2:

Quasi-LPV Decay Rate

OP7 (fixed K)**:**

$$\min_{Q,\, N} \text{trace}(N) : \begin{cases} (85),\ (86),\ \forall x \in \mathcal{V}_{\bar{\mathcal{X}}},\ \forall \delta \in \mathcal{V}_{\Delta} \\ \begin{bmatrix} Q & I \\ I & N \end{bmatrix} \succeq 0 \end{cases} \tag{98}$$

OP8 (fixed P)**:**

$$\min_{K,\, N} |\text{trace}(\Lambda)| : \begin{cases} (85),\ \forall x \in \mathcal{V}_{\bar{\mathcal{X}}},\ \forall \delta \in \mathcal{V}_{\Delta} \\ \begin{bmatrix} Q & I \\ I & N \end{bmatrix} \succeq 0 \end{cases} \tag{99}$$

where Λ is the resulting matrix on the left side of equation (85).

DAR Decay Rate

OP9 (fixed K)**:**

$$\min_{Q,\, W_1,\, W_2,\, N} \text{trace}(N) : \begin{cases} (91),\ (92),\ \forall x \in \mathcal{V}_{\bar{\mathcal{X}}},\ \forall \delta \in \mathcal{V}_{\Delta} \\ \begin{bmatrix} Q & I \\ I & N \end{bmatrix} \succeq 0 \end{cases} \tag{100}$$

OP10 (fixed P)**:**

$$\min_{K,\, W_1,\, N} |\text{trace}(\Lambda)| : \begin{cases} (91),\ \forall x \in \mathcal{V}_{\bar{\mathcal{X}}},\ \forall \delta \in \mathcal{V}_{\Delta} \\ \begin{bmatrix} Q & I \\ I & N \end{bmatrix} \succeq 0 \end{cases} \tag{101}$$

where Λ is the resulting matrix on the left side of equation (91).

4.6.2 Reduced Oscillation

Considering the same system described for Problem 4.1:

Problem 4.3. *Determine a static output feedback control law that maximizes the estimate of the region of attraction, inside a specified domain of interest, in which every initial state approaches the origin asymptotically at a decay rate of at least σ, limiting the imaginary part of the eigenvalues of the closed-loop system's linear portion to $\pm\nu$.*

This additional restriction on the linear part's eigenvalues has the objective of reducing the oscillatory behavior of the system's response, which will be referred hereafter as constrained oscillatory behavior.

As additional tools to solve such performance extension of the original problem, the definition of LMI regions and $\mathcal{D}$-stability are now introduced according to (MACKENROTH, 2004).

Definition 4.2. (LMI Regions) *A subset $\mathcal{D}$ is called an LMI region if there exists a symmetric $m \times m$-matrix L and an arbitrary $m \times m$-matrix M such that:*

$$\mathcal{D} = \left\{ z \in \mathbb{C} : L + zM + \bar{z}M^{\intercal} < 0 \right\} \tag{102}$$

The matrix-valued function

$$f_{\mathcal{D}}(z) = L + zM + \bar{z}M^{\intercal} \tag{103}$$

is denoted as the characteristic function of $\mathcal{D}$.

Definition 4.3. ($\mathcal{D}$-stability) *A matrix A is called $\mathcal{D}$-stable if all its eigenvalues lie in $\mathcal{D}$.*

It is important to note that, although the $\mathcal{D}$-stability is defined for linear systems, applying it on the hereby called "linear part" of the nonlinear system under study brings the possibility of achieving relevant performance improvements.

Considering that, the following horizontal band LMI region is defined as a restriction to the imaginary part of the eigenvalues of the set of linearized closed-loop feedback for all vertices assessed. According to the format in (CHADLI; BORNE; DUBUISSON, 2012), for square matrices A and X, with z as the eigenvalues of A, and a positive scalar ν:

$$\mathcal{S} = \left\{ z \in \mathbb{C} : |\operatorname{Im}(z)| < \nu \Leftrightarrow \begin{bmatrix} -2\nu & z - \bar{z} \\ -z + \bar{z} & -2\nu \end{bmatrix} < 0 \right\} \tag{104}$$

which gives the following LMI restriction:

$$\begin{bmatrix} -2\nu X & AX - (AX)^{\intercal} \\ -AX + (AX)^{\intercal} & -2\nu X \end{bmatrix} \prec 0 \tag{105}$$

Therefore, given the definitions above, the domain of interest $\mathcal{X}$ in (48) and polytopes $\bar{\mathcal{X}}$ in (57) and Δ in (60), and also the LMI region in (104), the following theorems,

adapted from (CASTRO, 2019), address the asymptotic stability with exponential performance and constrained oscillatory behavior of the closed-loop 2D camera system.

Theorem 5. (Quasi-LPV Reduced Oscillation) *Considering the Quasi-LPV representation* (32) *of system* (23) *and letting* (44) *be the static output feedback control law for the closed-loop system: Suppose there are matrices* $K \in \mathbb{R}^{m\times n}$ *and* $Q = Q^\intercal \succeq 0 \in \mathbb{R}^{n\times n}$ *and positive scalars* $\sigma \in \mathbb{R}, \nu \in \mathbb{R}$ *such that for all* (x, δ) *evaluated at the convex set of vertices* $\mathcal{V}_{\bar{\mathcal{X}}} \times \mathcal{V}_\Delta$*:*

$$He\{(A(x,\delta) + BKC(x,\delta))Q + \sigma Q\} \prec 0 \tag{106}$$

$$\begin{bmatrix} Q & Q \\ Q & \Upsilon \end{bmatrix} \succeq 0 \tag{107}$$

$$\begin{bmatrix} -2\nu Q & FQ - (QF)^\intercal \\ -FQ + (QF)^\intercal & -2\nu Q \end{bmatrix} \prec 0 \tag{108}$$

where $F = A(x,\delta) + BKC(x,\delta)$.

Then, all closed-loop trajectories starting in $\mathcal{R}$ *asymptotically approach the origin at a decay rate of at least* σ *with oscillation constrained by* ν *in the imaginary part of the eigenvalues of* F*, being this region of attraction estimate defined as:*

$$\mathcal{R} = \{x \in \mathbb{R}^n : x^\intercal P x \leq 1\} \subset \mathcal{X} \tag{109}$$

where $P = Q^{-1}$.

Proof: Taking credit from the proof for Theorem 1, which demonstrates how the asymptotic stability criteria are transformed into a set of conditions based on matrix inequalities, and Theorem 3, which demonstrates how to guarantee a specified decay rate for $\dot{V}(x)$, the constrained oscillation of the dynamic behavior of the system response is achieved by restricting the eigenvalues of $F = A(x,\delta) + BKC(x,\delta)$ to a horizontal band with limits on the imaginary part at $[-\nu, \nu]$.

Assuming the additional restriction (108) is the LMI condition (similar to (105)) for F to be $\mathcal{D}$-stable (see Definition 4.3) in the $\mathcal{S}$ domain (104), respecting then the characteristic function inside the domain definition, then according to Definition 4.2, $\mathcal{S}$ can be considered an LMI region where the eigenvalues of $F = A(x,\delta) + BKC(x,\delta)$ lie. This verifies, therefore, the reduced oscillation requirement of Problem 4.3.

Theorem 6. (DAR Reduced Oscillation) *Considering the DAR representation* (36) *of system* (23) *and letting* (44) *be the static output feedback control law for the closed-loop system: Suppose there are matrices* $K \in \mathbb{R}^{m\times n}$*,* $Q = Q^\intercal \succeq 0 \in \mathbb{R}^{n\times n}$*,* $W_1 \in \mathbb{R}^{n_\xi \times n_\xi}$ *and* $W_2 \in \mathbb{R}^{n_\pi \times n_\pi}$ *and positive scalars* $\sigma \in \mathbb{R}, \nu \in \mathbb{R}$ *such that for all* (x, δ) *evaluated at the*

convex set of vertices $\mathcal{V}_{\bar{\mathcal{X}}} \times \mathcal{V}_{\Delta}$:

$$\begin{bmatrix} He\{(A_1(\delta) + B_1KC_1(\delta))Q + \sigma Q\} & A_2(\delta)W_1^{\intercal} + Q\Omega_1^{\intercal}(x) & (B_1KC_2(\delta))W_2^{\intercal} + Q\Pi_1^{\intercal}(x) \\ & He\{\Omega_2 W_1^{\intercal}\} & 0 \\ \star & & He\{\Pi_2 W_2^{\intercal}\} \end{bmatrix} \prec 0 \tag{110}$$

$$\begin{bmatrix} Q & Q \\ Q & \Upsilon \end{bmatrix} \succeq 0 \tag{111}$$

$$\begin{bmatrix} -2\nu Q & FQ - (QF)^{\intercal} \\ -FQ + (QF)^{\intercal} & -2\nu Q \end{bmatrix} \prec 0 \tag{112}$$

where $F = A_1(\delta) + B_1KC_1(\delta)$.

Then, all closed-loop trajectories starting in $\mathcal{R}$ asymptotically approach the origin at a decay rate of at least σ with oscillation constrained by ν in the imaginary part of the eigenvalues of F, being this region of attraction estimate defined as:

$$\mathcal{R} = \{x \in \mathbb{R}^n : x^{\intercal}Px \leq 1\} \subset \mathcal{X} \tag{113}$$

where $P = Q^{-1}$.

Proof: Taking credit from the proof for Theorem 2, which demonstrates how the asymptotic stability criteria are transformed into a set of conditions based on matrix inequalities, and Theorem 4, which demonstrates how to guarantee a specified decay rate for $\dot{V}(x)$, the constrained oscillation of the dynamic behavior of the system response is achieved by restricting the eigenvalues of $F = A_1(\delta) + B_1KC_1(\delta)$ to a horizontal band with limits on the imaginary part at $[-\nu, \nu]$.

In a similar approach of the proof for Theorem 5, assuming the additional restriction (112) is the LMI condition (similar to (105)) for F to be $\mathcal{D}$-stable (see Definition 4.3) in the $\mathcal{S}$ domain (104), respecting then the characteristic function inside the domain definition, then according to Definition 4.2, $\mathcal{S}$ can be considered an LMI region where the eigenvalues of $F = A_1(\delta) + B_1KC_1(\delta)$ lie. This verifies, therefore, the reduced oscillation requirement of Problem 4.3.

Again, as done in the decay rate performance extension, considering the proposed Theorems 5 and 6, in a similar process as explained before in 4.5, they are turned into optimization problems to maximize the estimation of the region of attraction, in which the P-K iterative algorithm (EL GHAOUI; BALAKRISHNAN, 1994; SADABADI; PEAUCELLE, 2016) is used. For that, the same initial estimation for K is taken as in (79), based on the solution of (78).

With that, it is possible to define the following optimization problems with the objective of maximizing the region of attraction estimate considering Quasi-LPV and DAR representations, regarding Problem 4.3:

Quasi-LPV Reduced Oscillation

OP11 (fixed K)**:**

$$\min_{Q,\,N} \text{trace}(N) : \begin{cases} (106),\ (107),\ (108),\ \forall x \in \mathcal{V}_{\bar{\mathcal{X}}},\ \forall \delta \in \mathcal{V}_{\Delta} \\ \begin{bmatrix} Q & I \\ I & N \end{bmatrix} \succeq 0 \end{cases} \tag{114}$$

OP12 (fixed P)**:**

$$\min_{K,\,N} |\text{trace}(\Lambda)| : \begin{cases} (106),\ (108),\ \forall x \in \mathcal{V}_{\bar{\mathcal{X}}},\ \forall \delta \in \mathcal{V}_{\Delta} \\ \begin{bmatrix} Q & I \\ I & N \end{bmatrix} \succeq 0 \end{cases} \tag{115}$$

where Λ is the resulting matrix on the left side of equation (106).

DAR Reduced Oscillation

OP13 (fixed K)**:**

$$\min_{Q,\,W_1,\,W_2,\,N} \text{trace}(N) : \begin{cases} (110),\ (111),\ (112),\ \forall x \in \mathcal{V}_{\bar{\mathcal{X}}},\ \forall \delta \in \mathcal{V}_{\Delta} \\ \begin{bmatrix} Q & I \\ I & N \end{bmatrix} \succeq 0 \end{cases} \tag{116}$$

OP14 (fixed P)**:**

$$\min_{K,\,W_1,\,N} |\text{trace}(\Lambda)| : \begin{cases} (110),\ (112),\ \forall x \in \mathcal{V}_{\bar{\mathcal{X}}},\ \forall \delta \in \mathcal{V}_{\Delta} \\ \begin{bmatrix} Q & I \\ I & N \end{bmatrix} \succeq 0 \end{cases} \tag{117}$$

where Λ is the resulting matrix on the left side of equation (110).

5 NUMERICAL RESULTS

Some numerical results are presented in this chapter, in order to verify the control design described as a solution to each of the problems proposed in chapter 4.

The simulations were performed using Matlab software, with Yalmip toolbox for the optimization problems (LOFBERG, 2004). The solvers used in Yalmip were SDPT3 and SEDUMI.

5.1 General Definitions

Aiming at a more direct comparison of the results, some constant parameters were set to the same values in all simulations, as presented in (118), being them the intrinsic parameters of the camera and its moment of inertia in both axis, X and Y. Additionally, a 35mm focal distance was used, with a standard resolution of 1280×1024 pixels on the display. In accordance with these parameters, the camera FOV becomes $54.432° \times 37.849°$.

$$K_c = \begin{bmatrix} 1244.4 & 0 & 640 \\ 0 & 1493.3 & 512 \\ 0 & 0 & 1 \end{bmatrix} \quad J = \begin{bmatrix} 1 & 0 & 0 \\ 0 & 1 & 0 \\ 0 & 0 & 1 \end{bmatrix} \tag{118}$$

Although it is straightforward to compare some quantitative aspects of the results, such as the trace of the resulting matrix P, which translates into a smaller or larger estimate of the region of attraction, and the settling time obtained for each error norm response, which can be used to verify an approximate decay rate of the error, some qualitative aspects are also evaluated so that it is possible to make a complete analysis of the results.

Note that the criteria used for estimating the settling time is as follows: considering the initial error norm between the desired final position for the feature on the display and its initial position is 100%, the settling time is the time the feature takes to depart from this initial position and attain (also staying within) 2% of the initial error.

Finally, two kinds of results are obtained, the first one related to the optimization problem (achieved K and P matrices and the estimation of the region of attraction), and

another consisting of the dynamic response of the system over time. For the optimization problems, a set of 10 P-K iterations was considered reasonable. Also, for better comparison of results, some input parameters were set to the same values in all simulations, being them:

Desired angular range on the camera field of view (see section 4.3.1 item (a)):

$\psi_{\hat{X}} = 25.5° \quad \psi_{\hat{Y}} = 18.9°$

Initial *feature* projection: $300 \times 650\ px$

Desired *feature* projection: $670 \times 460\ px$

Restriction in ω was imposed to the domain of interest in addition to ϵ, as explained in section 4.3.1. It means that the system is analyzed for stability in a more restricted ω region (though still sufficient to enable adequate rotation speeds in each camera axis), therefore allowing a larger ϵ region to be acquired.

Regarding the initial conditions for the simulations, the initial and desired coordinates μ_c and $\bar{\mu}$ were obtained based on their projections m and $\bar{m}$ by inverting equation (29):

$$\mu_c = K_c^{-1} m \qquad \bar{\mu} = K_c^{-1} \bar{m} \tag{119}$$

Then, the rotation angle and vector are calculated, resulting in the quaternion initial conditions:

$$\begin{gathered} \psi_0 = \arccos \frac{\mu_c \cdot \bar{\mu}}{\|\mu_c\| \ \|\bar{\mu}\|} \qquad \vec{r}_0 = \frac{\mu_c \times \bar{\mu}}{\|\mu_c\| \ \|\bar{\mu}\| \sin \psi_0} \\ \epsilon_0 = \vec{r}_0 \sin(\tfrac{\psi_0}{2}) \end{gathered} \tag{120}$$

The initial conditions for rotation speed were set to $\omega_0 = \begin{bmatrix} 0 & 0 & 0 \end{bmatrix}^\intercal$.

5.2 Results for the General Asymptotic Stability Problem

The results from the general asymptotic stability problem (Problem 4.1) simulations are presented in this section. In figure 4, the outer green rectangle establishes the limits for the desired feature position. Inside it, an octagonal blue polytope where the vertices $\mathcal{V}_{\bar{\mathcal{X}}}$ of the polytope $\bar{\mathcal{X}}$ lie. Inside the octagon a blue ellipsoid marks the domain of interest $\mathcal{X}$. Finally, the red ellipsoid shows the RoA estimate obtained using Quasi-LPV representation and the green one shows the RoA estimate obtained using DAR. These regions were obtained considering $\omega = 0$.

Figure 5 has essentially the same information as figure 4, but showing the region of attraction estimate in terms of the quaternion coordinates ϵ_x and ϵ_y. It can also be seen in this figure a greater RoA estimate obtained with DAR than the one obtained with Quasi-LPV.

The control design problem was solved for both model representations, so that to compare the performance of the optimization for each representation, figure 6 shows the outline of the trace of P along each iteration.

Figure 4 – Image region of attraction estimate for stability problem.

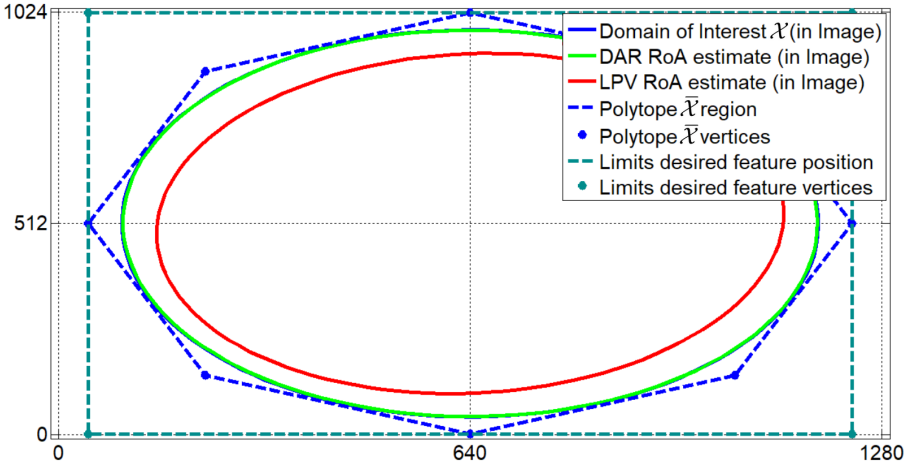

Source: from the author.

Figure 5 – Quaternion region of attraction estimate for stability problem.

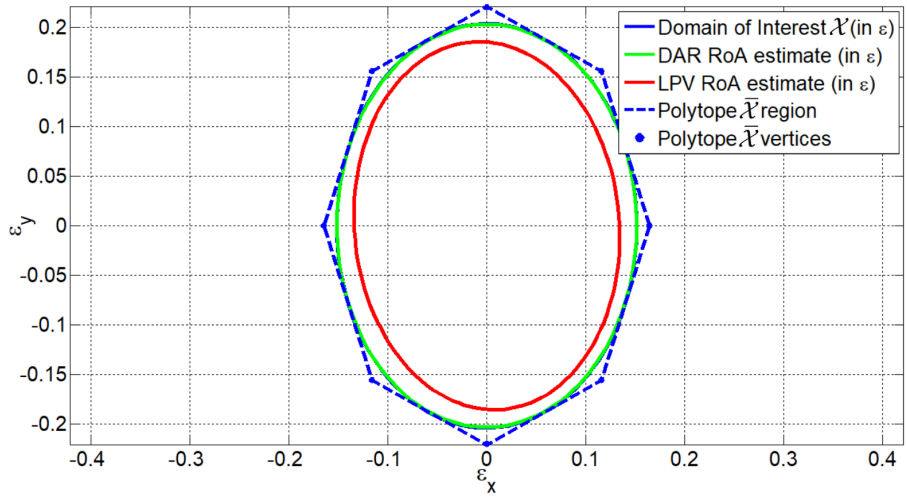

Source: from the author.

Figure 6 – Trace of P for stability problem.

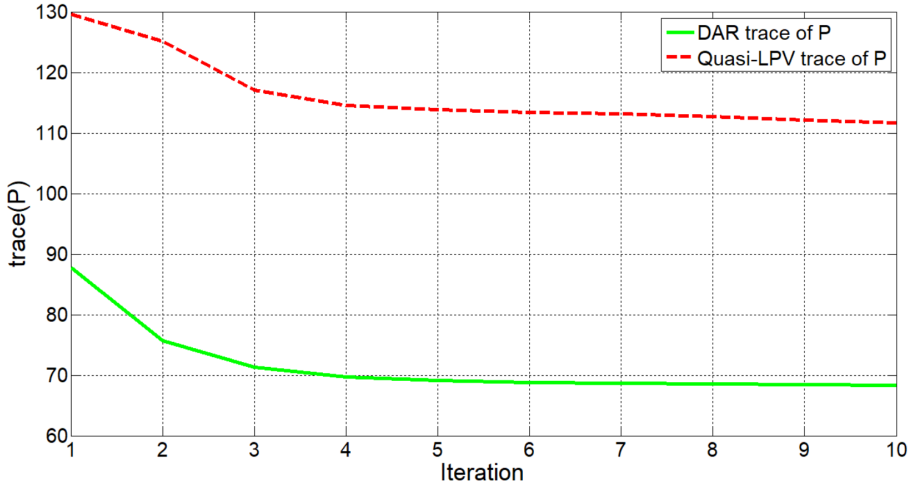

Source: from the author.

Considering that, for Quasi-LPV the final matrix P had $trace(P_{qLPV}) = 111.63$, being:

$$P_{qLPV} = \begin{bmatrix} 55.565 & 2.2685 & -0.46141 & 11.87 \\ 2.2685 & 29.09 & -8.4226 & 3.2123 \\ -0.46141 & -8.4226 & 15.108 & -2.2381 \\ 11.87 & 3.2123 & -2.2381 & 11.863 \end{bmatrix} \tag{121}$$

with the resulting output feedback gain K matrix:

$$K_{qLPV} = \begin{bmatrix} -0.00011751 & -2.7428 \times 10^{-05} & -0.36909 & 1.6358 \\ 2.4034 \times 10^{-05} & -9.2695 \times 10^{-05} & -2.2621 & 0.16179 \end{bmatrix} \tag{122}$$

For DAR, final matrix P had $trace(P_{DAR}) = 68.319$ and the value:

$$P_{DAR} = \begin{bmatrix} 43.585 & -0.06493 & 0.0082866 & -0.15777 \\ -0.06493 & 24.199 & 0.16498 & 0.15213 \\ 0.0082866 & 0.16498 & 0.27875 & 0.094787 \\ -0.15777 & 0.15213 & 0.094787 & 0.25599 \end{bmatrix} \tag{123}$$

with K:

$$K_{DAR} = \begin{bmatrix} 0.005544 & -0.016127 & -26.066 & -47.543 \\ 0.0068577 & 0.012375 & 58.49 & 10.148 \end{bmatrix} \tag{124}$$

The next figures show the results for 100 seconds with the Quasi-LPV representation. In figure 7 the quaternion values ϵ_x and ϵ_y approach zero, as well as the image error in each display axis shown in figure 8, leading the *feature* to the target position. Both figures exhibit an oscillatory behavior which reflects in the *feature* trajectory. This oscillation becomes even more evident in figure 9 for the rotation speed components.

Figure 7 – Quasi-LPV ϵ (quaternion) for stability problem.

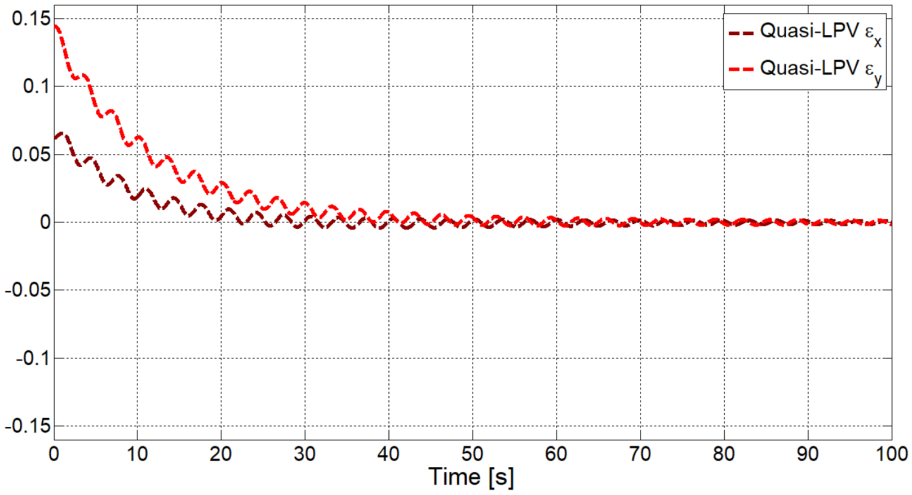

Source: from the author.

Figure 8 – Quasi-LPV image error for stability problem.

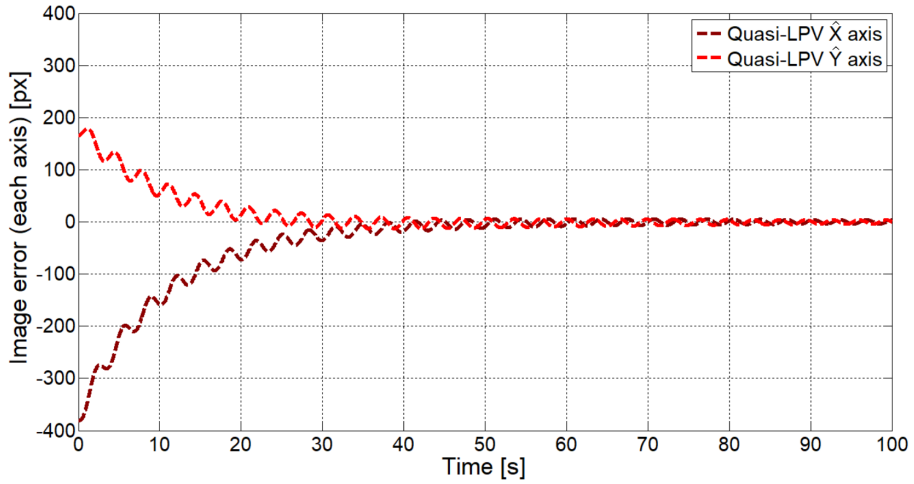

Source: from the author.

Figure 9 – Quasi-LPV system rotation speed for stability problem.

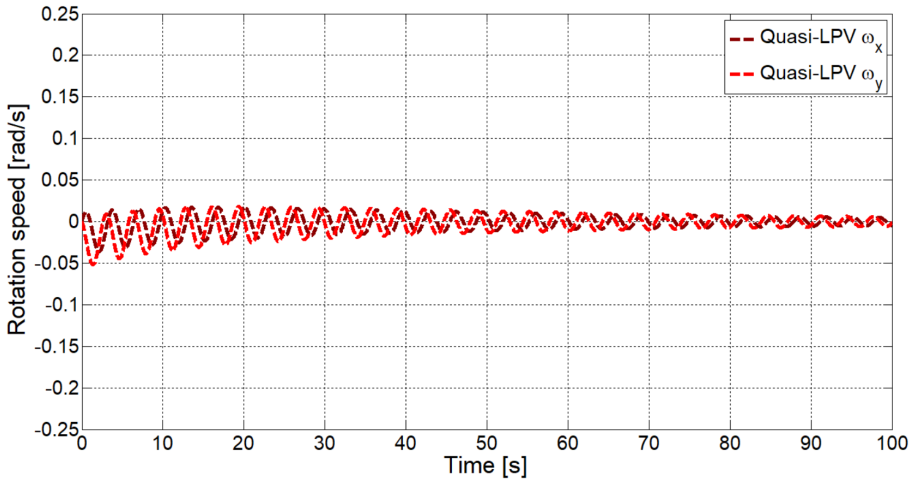

Source: from the author.

Following that, the DAR results for 100 seconds are shown. In figure 10 the quaternion values ϵ_x and ϵ_y approach zero, which happens also for the image error components in figure 11. This means that the *feature* approaches its desired position as expected. The oscillatory behavior is also present for the DAR, but far less expressive than in the Quasi-LPV simulation. Figure 12 evidences a strong fast initial bouncing in the rotation speed components ω_x and ω_y, which after some seconds considerably reduces.

Figure 13 shows that the image error norm in DAR decays faster than in Quasi-LPV, which can also be verified with the settling time for each of them: $T_{sqLPV} = 65.07s$ and $T_{sDAR} = 15.50s$.

Figure 14 shows the image projection path for both simulations, where the DAR shows a longer *feature* trajectory than the Quasi-LPV, although presenting lower levels of oscillation. Nevertheless, both met the objective of approaching asymptotically to the desired position.

Figure 10 – DAR ϵ (quaternion) for stability problem.

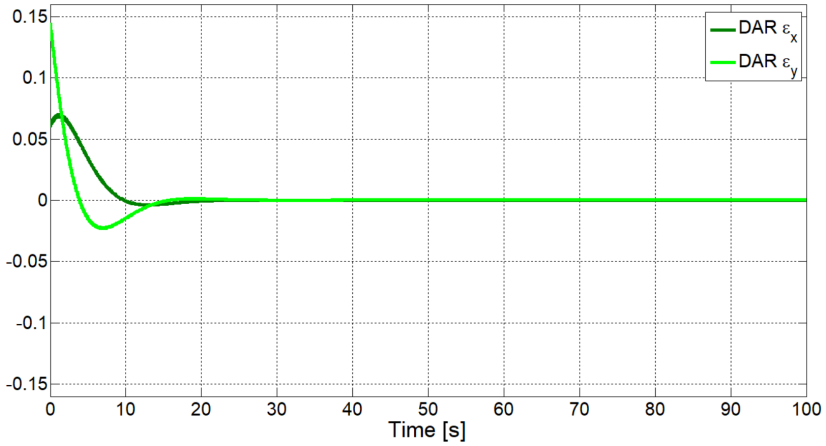

Source: from the author.

Figure 11 – DAR image error for stability problem.

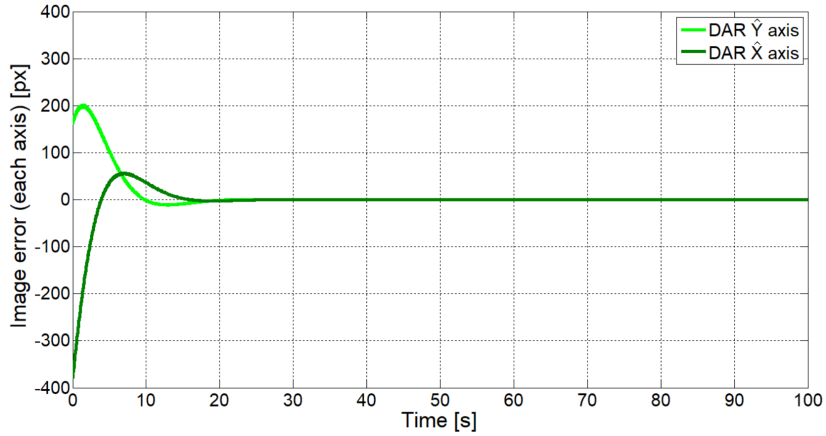

Source: from the author.

Figure 12 – DAR system rotation speed for stability problem.

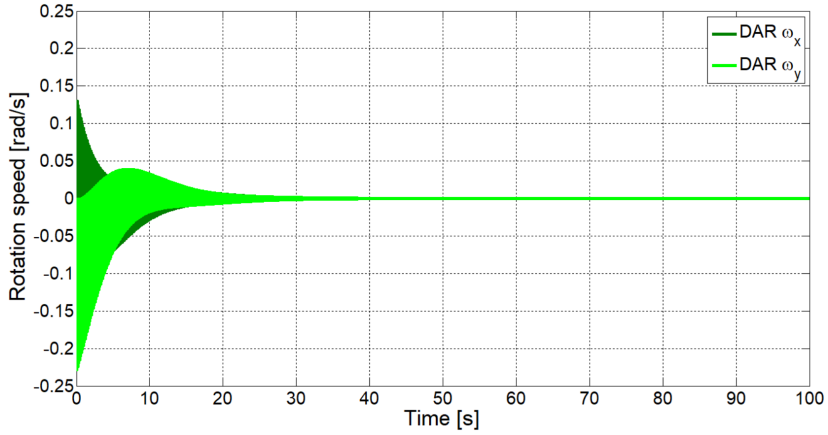

Source: from the author.

Figure 13 – Image error norm for stability problem.

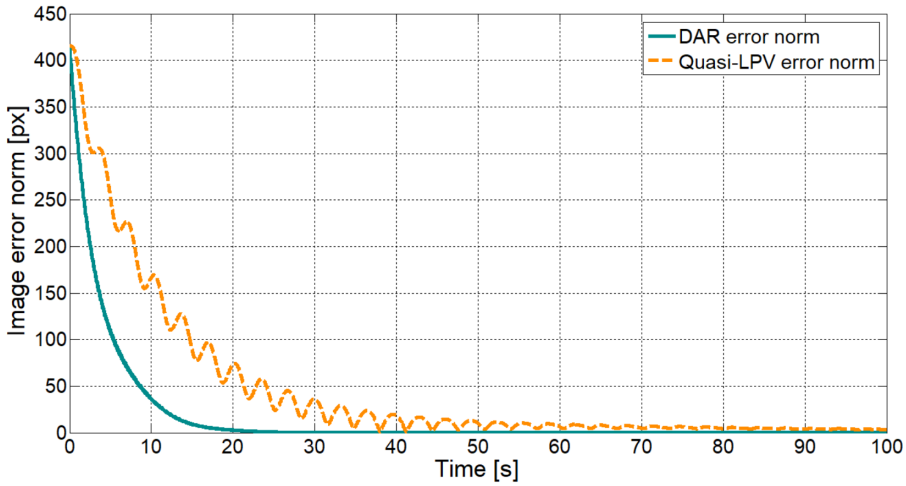

Source: from the author.

Figure 14 – Image projection path for stability problem.

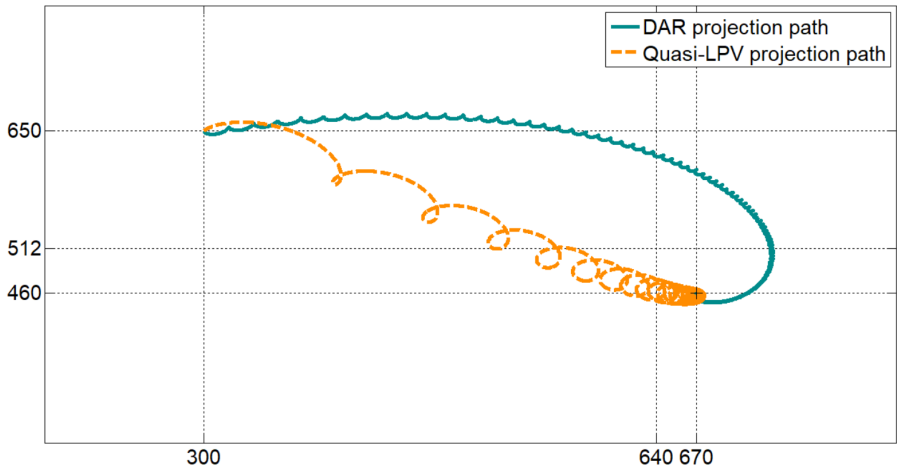

Source: from the author.

5.3 Stabilization Problem with Exponential Decay of the Error

This section shows simulation results from the asymptotic stabilization problem with an exponential decay constraint (Problem 4.2). All parameters from the general stabilization problem where maintained, with the addition of:

Minimum exponential decay rate: $\sigma = 0.25$

With that, the resulting RoA estimate for DAR (in green) and Quasi-LPV (in red) are shown in figure 15, which evidences a slightly greater region estimate for the DAR. This is a result of the evolution of the trace of P along 10 iterations of the optimization algorithm for each model representation, presented in figure 16.

Figure 15 – Image region of attraction estimate - decay constraint.

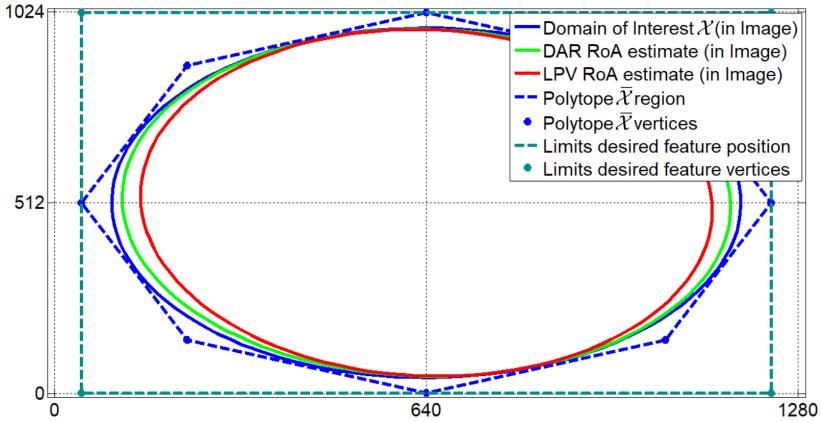

Source: from the author.

Figure 16 – Trace of P - decay constraint.

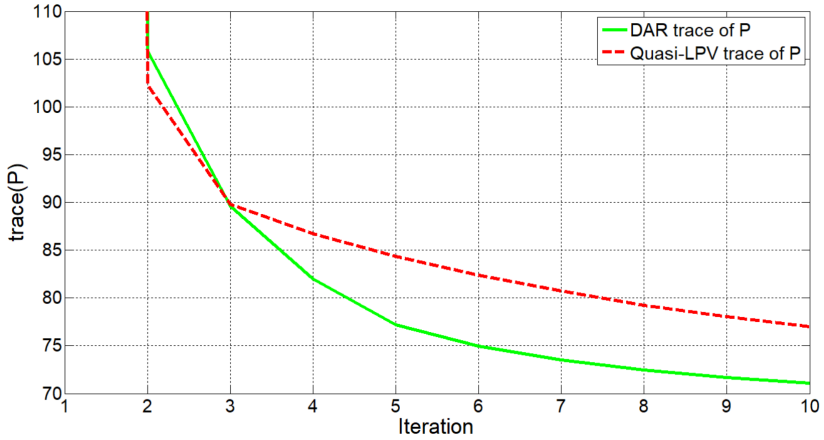

Source: from the author.

For Quasi-LPV, final matrix P had $trace(P_{dqLPV}) = 76.966$ and the value:

$$P_{dqLPV} = \begin{bmatrix} 44.199 & -1.3753 & 0.85141 & -1.2197 \\ -1.3753 & 28.571 & -2.1768 & 3.6602 \\ 0.85141 & -2.1768 & 1.183 & -1.8257 \\ -1.2197 & 3.6602 & -1.8257 & 3.0127 \end{bmatrix} \tag{125}$$

and the resulting output feedback gain matrix K was:

$$K_{dqLPV} = \begin{bmatrix} 0.067555 & -0.08741 & 30.786 & -55.862 \\ 0.042874 & -0.051461 & 21.423 & -36.448 \end{bmatrix} \tag{126}$$

For DAR, final matrix P had $trace(P_{dDAR}) = 71.091$ and the value:

$$P_{dDAR} = \begin{bmatrix} 44.072 & -0.81816 & 0.54818 & -0.64084 \\ -0.81816 & 25.523 & -0.69051 & 1.1889 \\ 0.54818 & -0.69051 & 0.51923 & -0.53651 \\ -0.64084 & 1.1889 & -0.53651 & 0.97749 \end{bmatrix} \tag{127}$$

with K:

$$K_{dDAR} = \begin{bmatrix} 0.020003 & -0.029058 & -8.7616 & -10.021 \\ 0.01802 & -0.014872 & 2.3292 & -13.573 \end{bmatrix} \tag{128}$$

The next figures show the Quasi-LPV results for 10 seconds of simulation time. In figure 17, the quaternion values ϵ_x and ϵ_y approach zero. The same for the image error along each display axis presented in figure 18. It becomes evident that the decay rate is considerably faster than the one verified in the general stability problem, being necessary only 10 seconds of simulation to verify the settling of the data. In figure 19, the rotation speed components ω_x and ω_y have shown the same decay pattern.

Figure 17 – Quasi-LPV ϵ (quaternion) - decay constraint.

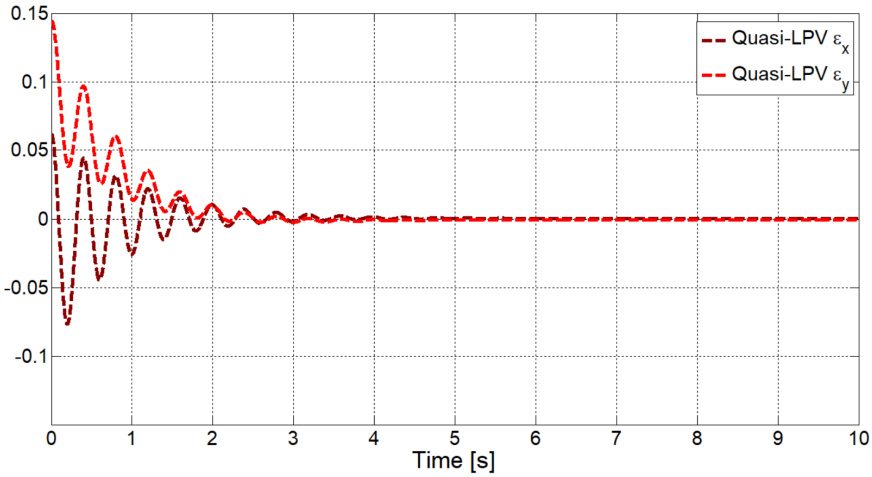

Source: from the author.

Figure 18 – Quasi-LPV image error - decay constraint.

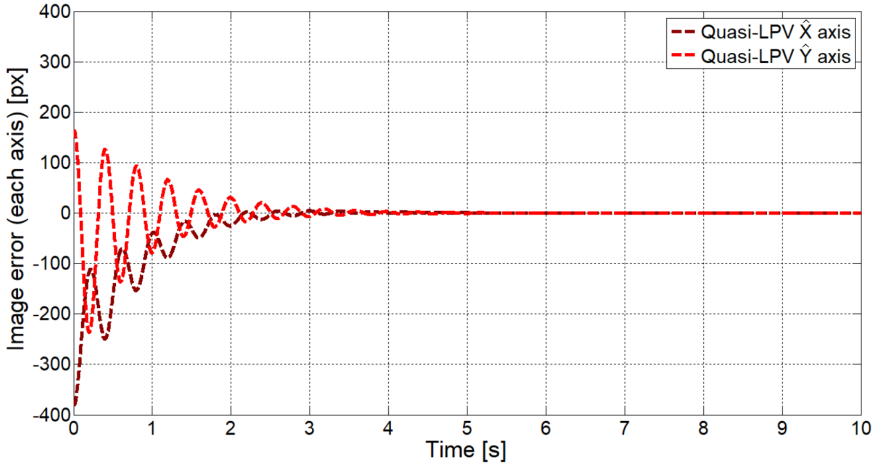

Source: from the author.

Figure 19 – Quasi-LPV system rotation speed - decay constraint.

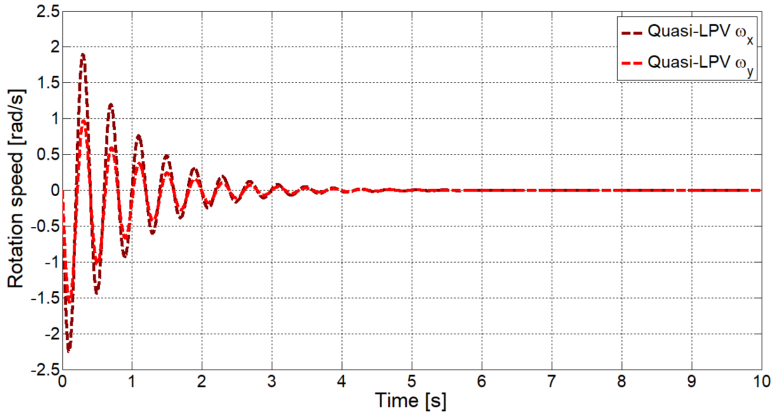

Source: from the author.

The DAR results for 10 seconds are shown in figures 20, 21 and 22, where a similar decay rate increase is verified, although exhibiting less oscillatory behavior than the simulation with the Quasi-LPV model representation.

Figure 20 – DAR ϵ (quaternion) - decay constraint.

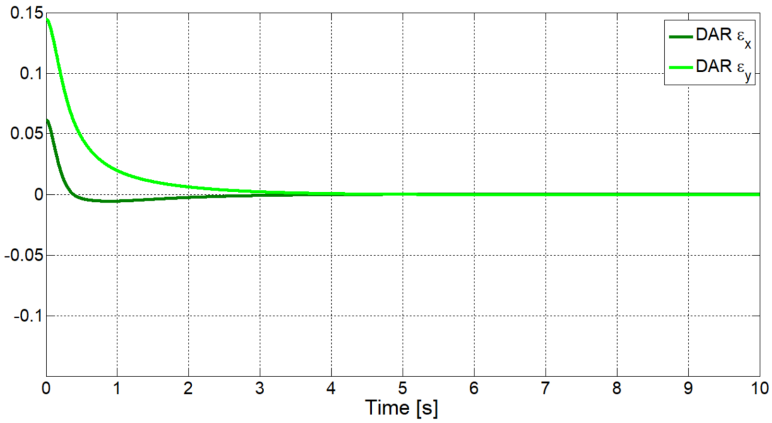

Source: from the author.

Figure 21 – DAR image error - decay constraint.

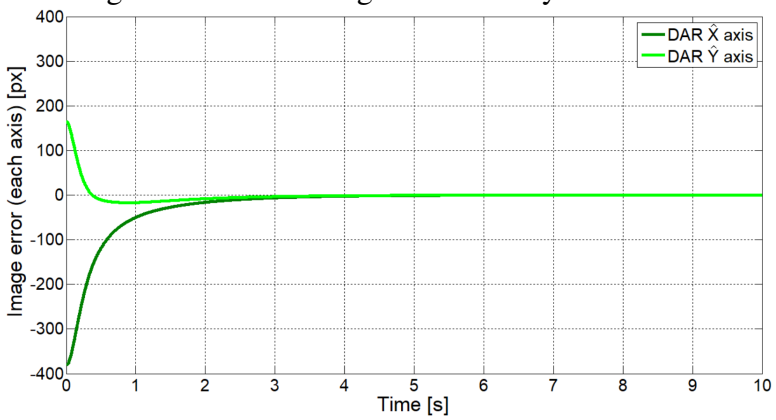

Source: from the author.

Figure 22 – DAR system rotation speed - decay constraint.

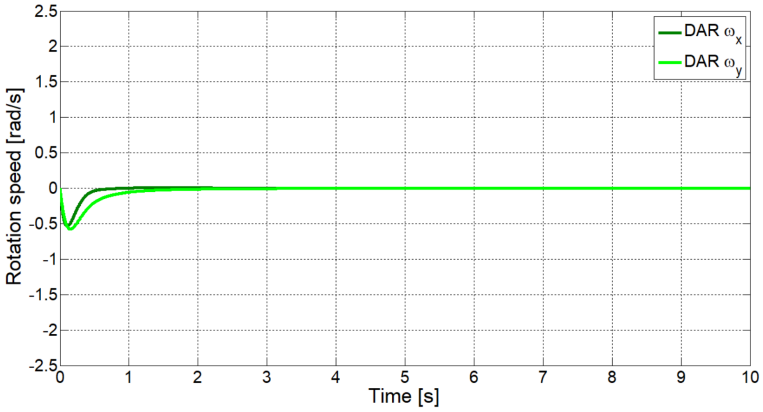

Source: from the author.

In figures 23 and 24 the image error norm and the image projection path are presented, respectively, for both cases. There is some bouncing present in the Quasi-LPV error norm, which can be better understood by checking the path profile. The DAR simulation shows a reduction on trajectory length to reach the target. The settling times were $T_{sdqLPV} = 3.204s$ and $T_{sdDAR} = 2.808s$, with DAR approaching the target faster than Quasi-LPV.

Figure 23 – Image error norm - decay constraint.

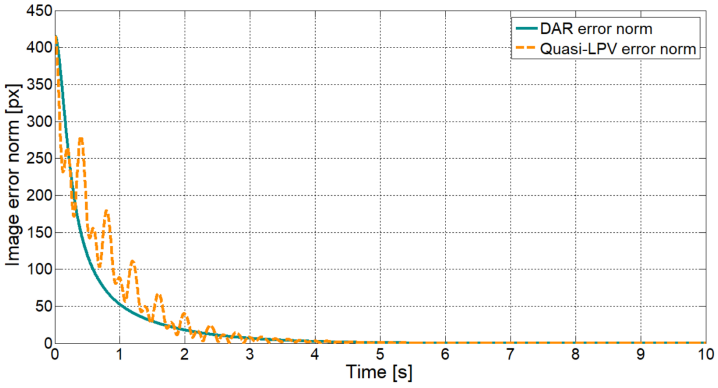

Source: from the author.

Figure 24 – Image projection path - decay constraint.

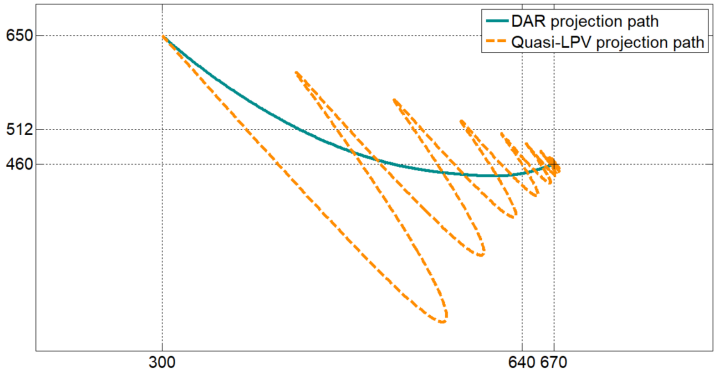

Source: from the author.

5.4 Stabilization Problem with Additional Oscillation Constraint

This section shows results from the optimization problem with exponential decay constraint and an additional oscillation constraint (Problem 4.3). These constraints are expressed as:

Minimum exponential decay rate: $\sigma = 0.25$

Maximum closed-loop linear portion eigenvalues' imaginary absolute value: $\nu = 1.5$

Figure 25 shows the RoA estimate for DAR (in green) is again larger than the RoA estimate for Quasi-LPV (in red), which is corroborated by the trace of P evolution along the 10 optimization iterations performed, presented in figure 26.

Figure 25 – Image region of attraction estimate - decay and oscillation constraints.

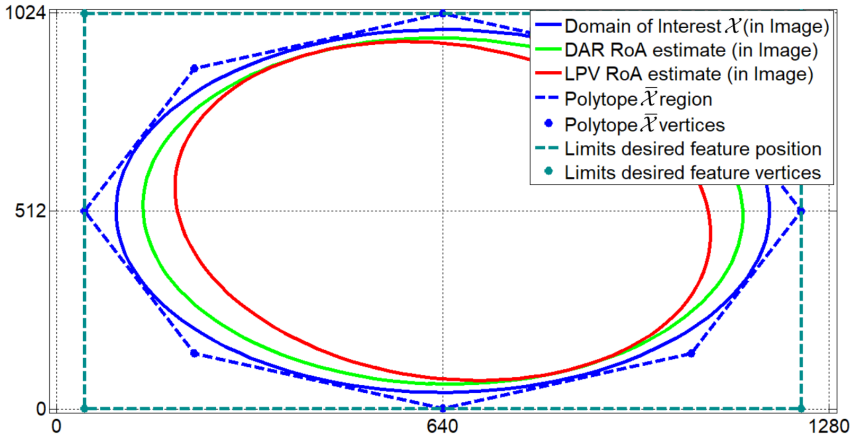

Source: from the author.

Figure 26 – Trace of P - decay and oscillation constraints.

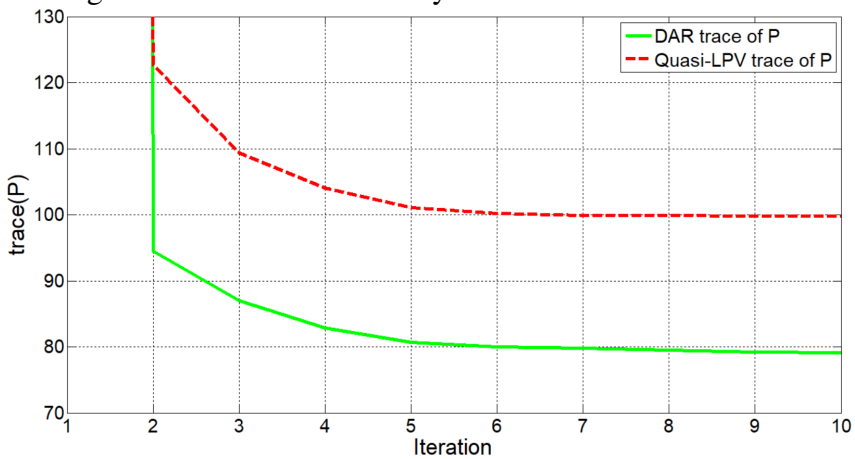

Source: from the author.

For Quasi-LPV, final matrix P had $trace(P_{oqLPV}) = 99.821$ and the value:

$$P_{oqLPV} = \begin{bmatrix} 50.256 & -5.249 & 6.5845 & -4.0415 \\ -5.249 & 34.95 & -5.3724 & 9.4124 \\ 6.5845 & -5.3724 & 6.4145 & -4.1794 \\ -4.0415 & 9.4124 & -4.1794 & 8.2 \end{bmatrix} \tag{129}$$

and the resulting output feedback matrix gain K was:

$$K_{oqLPV} = \begin{bmatrix} 0.00038725 & -0.0015794 & -2.8545 & 0.15989 \\ 0.0013654 & -0.00054789 & -0.4914 & -1.7584 \end{bmatrix} \tag{130}$$

For DAR, $trace(P_{oDAR}) = 79.073$, with P:

$$P_{oDAR} = \begin{bmatrix} 47.471 & -0.86038 & 2.2994 & -1.165 \\ -0.86038 & 28.043 & -1.0993 & 2.8452 \\ 2.2994 & -1.0993 & 1.4378 & -1.0812 \\ -1.165 & 2.8452 & -1.0812 & 2.1209 \end{bmatrix} \tag{131}$$

and the resulting output feedback matrix was:

$$K_{oDAR} = \begin{bmatrix} 0.0023996 & -0.0070236 & -14.977 & -2.0989 \\ 0.0042907 & -0.002881 & -6.096 & -5.8284 \end{bmatrix} \tag{132}$$

The next figures show a 10 second result for Quasi-LPV. In figure 27 the quaternion values ϵ_x and ϵ_y are presented, approaching zero. Figure 28 shows the image error along $\hat{X}$ and $\hat{Y}$ axis. In both figures it can be verified that the oscillatory behavior is considerably reduced in relation to the previous problems' results. In figure 29, the rotation speed components ω_x and ω_y are shown.

Figure 27 – Quasi-LPV ϵ (quaternion) - decay and oscillation constraints.

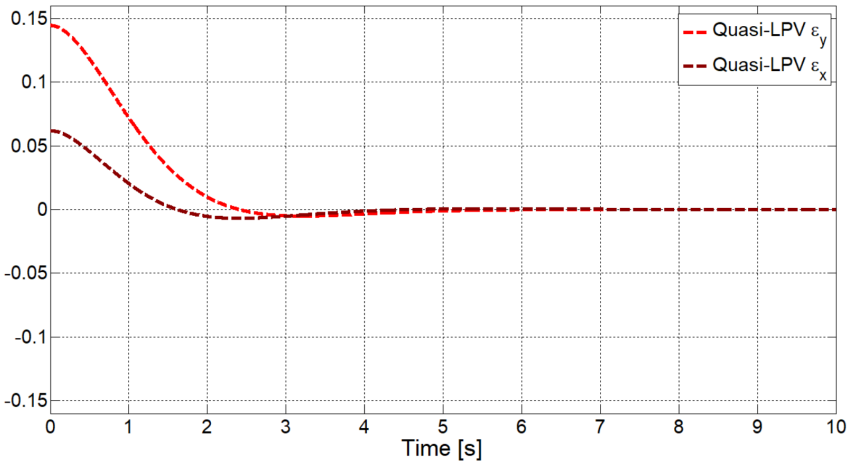

Source: from the author.

Figure 28 – Quasi-LPV image error - decay and oscillation constraints.

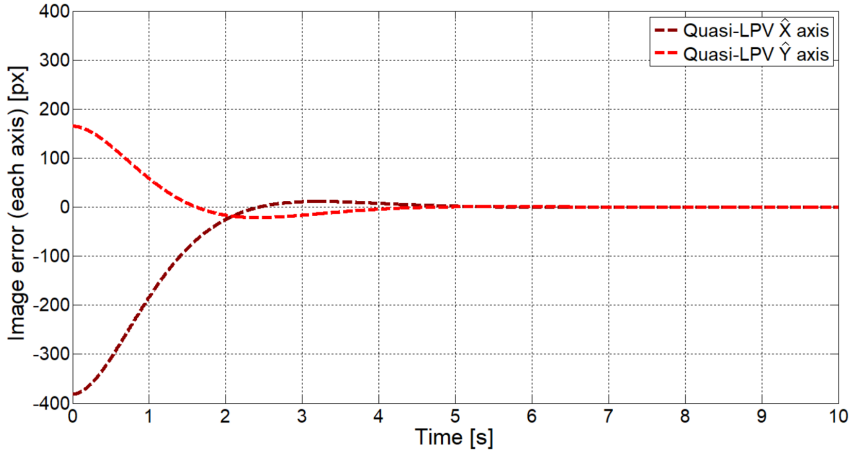

Source: from the author.

Figure 29 – Quasi-LPV system rotation speed - decay and oscillation constraints.

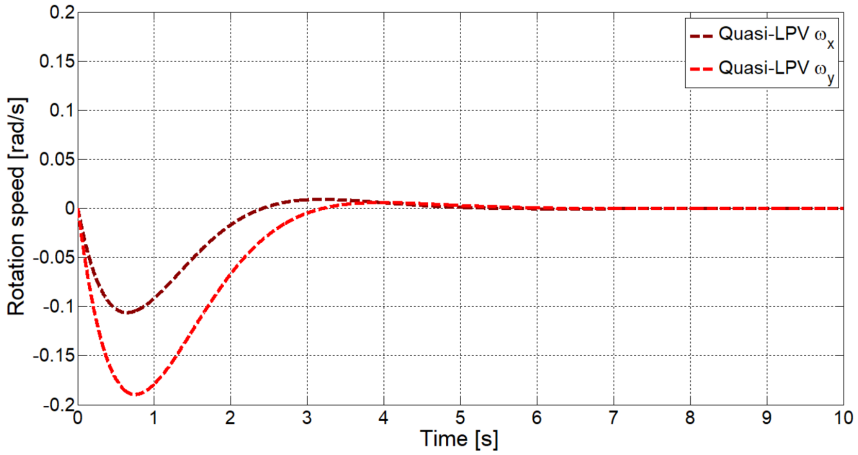

Source: from the author.

The DAR results are presented for 10 seconds of simulation time in the following figures. In figure 30 the quaternion values ϵ_x and ϵ_y approach zero, as expected considering the stability problem. Figure 31 shows the image error from the target position in pixels in $\hat{X}$ and $\hat{Y}$ axis. In both figures the behavior regarding decay rate and oscillation is similar to that obtained in Quasi-LPV results. Figure 32 shows the DAR rotation speed components ω_x and ω_y.

Figure 33 shows the image error norm of the Quasi-LPV and DAR simulations. It is possible to verify on it a lower oscillatory behavior than in the previous problems simulations. Regarding the image projection path, figure 34 shows a behavior that is consistent to the observations in previous figures for both representations. The estimated settling time for Quasi-LPV and DAR are, respectively, $T_{soqLPV} = 4.05s$, and $T_{soDAR} = 4.174s$.

Figure 30 – DAR ϵ (quaternion) - decay and oscillation constraints.

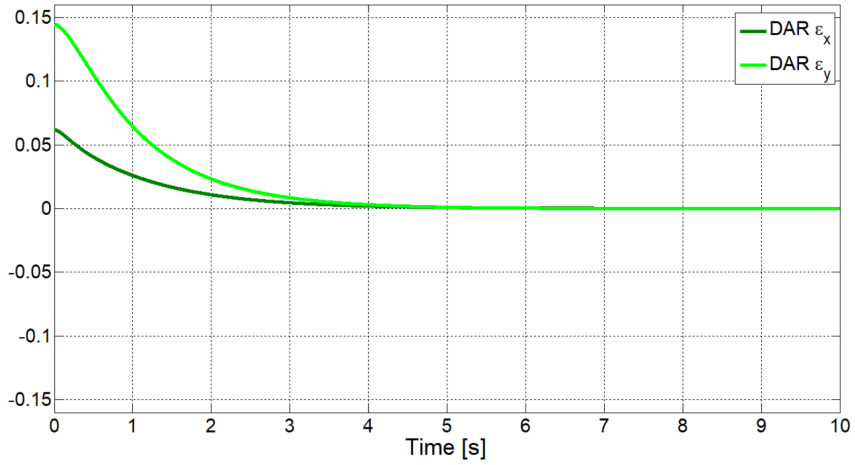

Source: from the author.

Figure 31 – DAR image error - decay and oscillation constraints.

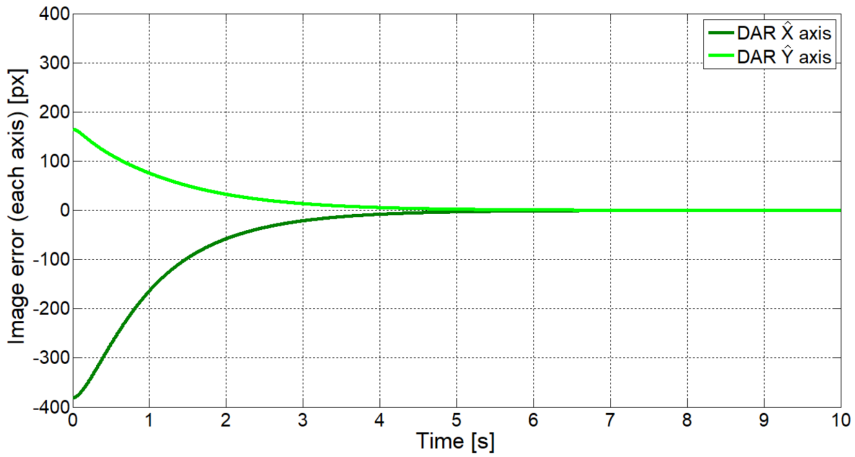

Source: from the author.

Figure 32 – DAR system rotation speed - decay and oscillation constraints.

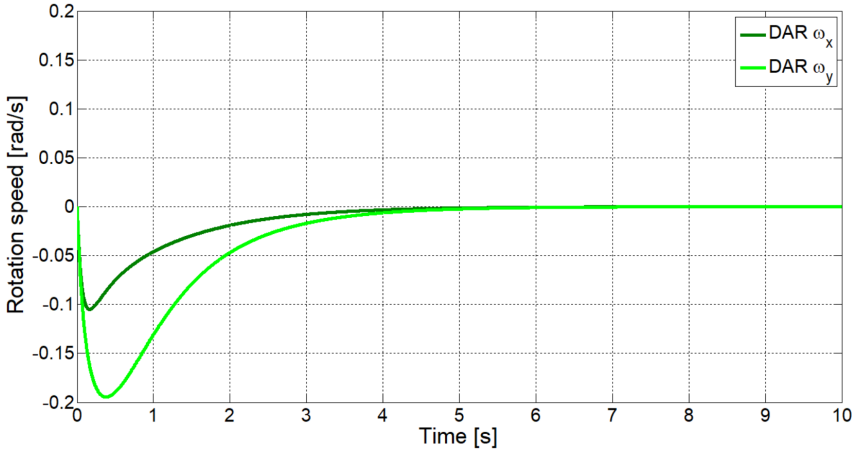

Source: from the author.

Figure 33 – Image error norm - decay and oscillation constraints.

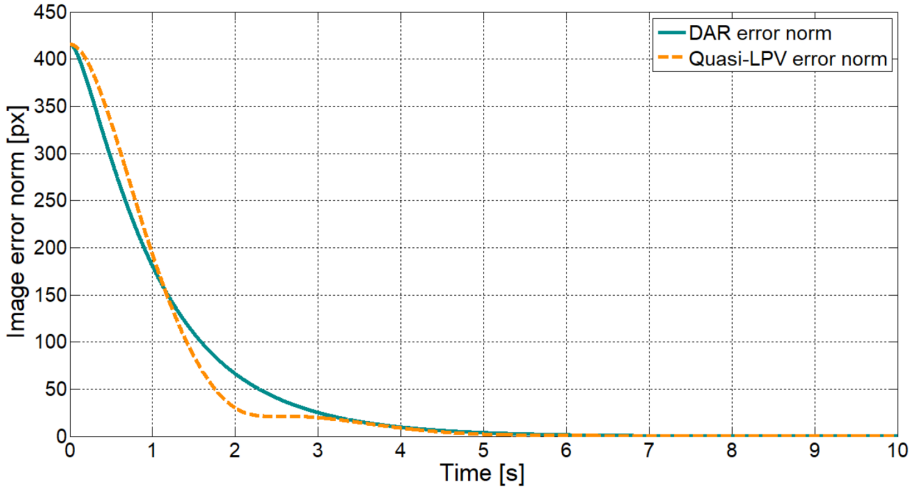

Source: from the author.

Figure 34 – Image projection path - decay and oscillation constraints.

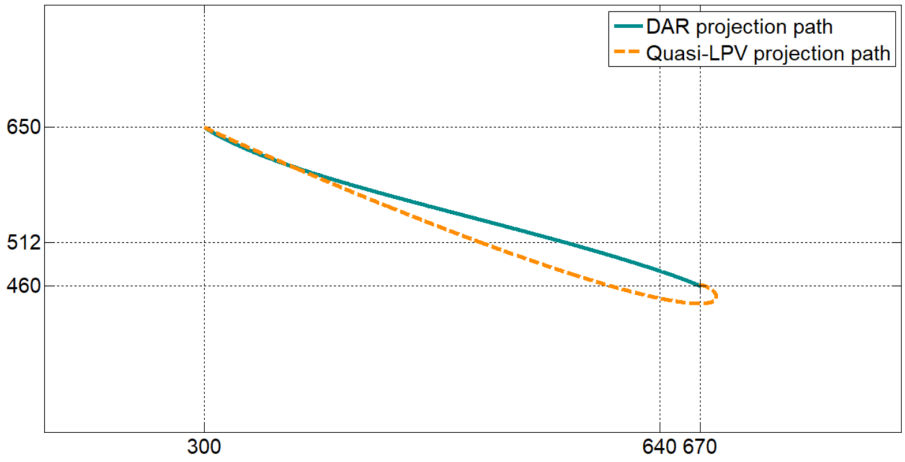

Source: from the author.

5.5 Final Analysis of the Simulation Results

The results obtained and presented along chapter 5 have provided examples that support the theoretic solutions which were developed and explained in chapter 4.

After analyzing the numerical results for the general asymptotic stability problem, it is possible to state that both Quasi-LPV and DAR solutions met the problem objective. By achieving a feasible solution for K and P, figures 13 and 14 show that the *feature* projection is successfully positioned at the desired coordinate.

Of course, these results are supported also by the figures that show, for each of the representations, the quaternion response, the image error on each axis along time and the rotation speed behavior. And, as expected, since this problem is unconstrained regarding decay rate and oscillation, there is a high settling time with an oscillatory behavior on the path of the feature. It can also be noted a better optimization of the region of attraction

estimate for the DAR in relation to the Quasi-LPV.

For the problem extension on exponential decay rate constraint, again figures 23 and 24, together with the settling time acquired, provide data that supports their objective achievement. Oscillation of the responses and trajectories are still high, mainly on the Quasi-LPV case. Again in this case the region of attraction estimated of the DAR is greater than for Quasi-LPV, as shown in figure 15 and supported by the numerical value of the trace of P for both.

Finally, the results of the extension for oscillation constraint provide, as it can be seen in figures 33 and 34, a less oscillatory response (more direct path for the desired *feature* image coordinate), and still a settling time compatible with the decay rate defined. As in previous cases, DAR had a larger estimation of the region of attraction in comparison to Quasi-LPV, as it can be seen in figure 25, and a lower value of trace of P, as shown in figure 26.

6 CONCLUSIONS

As stated in the introductory chapters, the main objective of this dissertation was to provide a systematic method for finding a static output feedback gain that stabilizes a closed-loop rigid-body dynamic system using the image output and the rotation speed. Theorems 1–6 presented in chapter 4 have provided conditions for the fulfillment of the requirements present in each of the problems proposed, while the optimization problems have guaranteed solutions which have as main outputs an SOF gain and an estimate of the region of attraction. Taking into account the simulation results which have verified both the methodology and the expected behavior for the system in each case, as a conclusion it can be considered that the main objective has been successfully achieved.

To accomplish that, some secondary objectives were not only necessary, but each of them has also generated interesting results that can be further studied. In chapter 3, the rigid-body rotation dynamic model used for the nonlinear camera system was represented both in a Quasi-LPV form and in a Differential Algebraic form. First, the 3-dimensional dynamic model was identified in both representations and then, considering the scope of the problems (related to a single image feature to have its image projection position controlled), it was simplified to 2-dimensional state-space models that served successfully for the control design proposed.

The definition of the outputs of the system, still part of chapter 3, was also an important part of the work performed, since it served as a basis for the static output feedback control employed on the system. While avoiding unnecessary complexity on the models, it also needed to be effective at providing the adequate response which could be viable considering the camera characteristics, thus, justifying the choice of taking an image-based error combined with the angular velocity in each axis. An additional advantage of this approach was to avoid having to measure directly the angular position. Then, based on some image formation concepts, described in chapter 2, the equations that were also introduced in each model representation were defined and explained.

In order to actually solve the stability problem, as well as the performance extensions proposed (*i.e.*, exponential decay rate and reduced oscillatory behavior), the background mathematical techniques introduced previously were used, as well as adaptations from

other authors' works referenced throughout the text. For the definition of a domain of interest that would provide an effective estimation of the region of attraction, both norm-based and polytopic approaches were combined resulting in a set of additional restrictions to the optimization problems.

On the optimization problems solution, it is important to note that since the theorems resulted in bilinear matrix inequalities, an iterative algorithm (called P-K) was used to transform the problem into step-by-step linear problems, which at each iteration kept improving its response by finding optimal gains to expand the estimated region of attraction for the asymptotic stable equilibrium point. Since this scheme was sensitive to the initial condition for the gain matrix, a first estimate of it was acquired with a linearization onto the equilibrium point studied (*i.e.*, the origin). Section 4.5 described in details how this process was performed.

Finally, as analyzed in section 5.5, the results obtained validate that the solutions proposed are satisfactory for the problems under the scenarios that were studied, being them: asymptotic stability, exponential decay and constrained oscillatory response.

Considering all that, the methods used in this work could potentially enhance the knowledge available on vision-based control systems and provide tools to develop real-world solutions in addition to the ones currently existing. Having that in mind, some future work on the subject is hereby proposed as a continuation of each main aspect studied in the present dissertation.

Additional research can be employed on refining the estimation of the region of attraction, by using for instance other functions to prove stability of the closed-loop system, with a format that suits the objective needs. Other extensions to the main stabilization problem can also be studied, such as input saturation, physical limits of the camera, and so on. Furthermore, extension to a 3-dimensional solution for the two-feature problem, which brings the necessity of assessing the third degree of freedom for the camera rotation as well as the definition of a combined output for the features' projection, would bring important evolution to the subject. Controlling the camera translation in addition to the rotation can also be a possible evolution, as well as the integration on practical applications.

REFERENCES

BOYD, S. *et al.* **Linear Matrix Inequalities in System and Control Theory**. Philadelphia, PA: SIAM, 1994.

BOYD, S.; VANDENBERGHE, L. **Convex Optimization**. Cambridge, UK: Cambridge University Press, 2004.

BRIAT, C. **Linear Parameter-Varying and Time-Delay Systems**. New York: Springer-Verlag Berlin Heidelberg, 2015. v. 3.

CASTRO, R. d. S. **Output Regulation of Rational Nonlinear Systems with Input Saturation**. 2019. Tese (Doutorado em Engenharia Elétrica) — Universidade Federal do Rio Grande do Sul, Porto Alegre, 2019.

CASTRO, R. S. *et al.* Controller and anti-windup code-sign for the output regulation of rational systems subject to control saturation. **International Journal of Robust and Nonlinear Control**, New Jersey, US, 2020.

CHADLI, M.; BORNE, P.; DUBUISSON, B. **Multiple Models Approach in Automation**. New Jersey, US: John Wiley Sons, Ltd, 2012. p. 161–166.

CHATURVEDI, N. A.; SANYAL, A. K.; MCCLAMROCH, N. H. Rigid-Body Attitude Control. **IEEE Control Systems Magazine**, ., v. 31, n. 3, p. 30–51, 2011.

COOK, S. The Importance of the P versus NP Question. **Journal of the ACM (JACM)**, New York, NY, USA, v. 50, n. 1, p. 27—-29, Jan. 2003.

COUTINHO, D. F. *et al.* Stability analysis and control of a class of differential-algebraic nonlinear systems. **International Journal of Robust and Nonlinear Control**, New Jersey, v. 14, n. 16, p. 1301–1326, 2004.

DAM, E. B.; KOCH, M.; LILLHOLM, M. **Quaternions, interpolation and animation**. .: Citeseer, 1998. v. 2.

DE FARIA, P. F. *et al.* Quaternion-based dynamic control of a 6-DOF Stewart Platform for periodic disturbance rejection. *In*: IEEE CONFERENCE ON CONTROL APPLICATIONS (CCA), 2016., 2016, . **Proceedings [...]** ., 2016. p. 1191–1196.

EL GHAOUI, L.; BALAKRISHNAN, V. Synthesis of fixed-structure controllers via numerical optimization. *In*: IEEE CONFERENCE ON DECISION AND CONTROL, 1994., 1994, . **Proceedings [...]** ., 1994. v. 3, p. 2678–2683.

GLEICHER, M.; WITKIN, A. Through-the-lens camera control. *In*: COMPUTER GRAPHICS AND INTERACTIVE TECHNIQUES, 19., 1992, . **Proceedings [...]** ., 1992. p. 331–340.

GRAUSTEIN, W. C. **Introduction to Higher Geometry**. New York: The Macmillan Company, 1930. (A series of mathematical texts).

HU, G. *et al.* Adaptive homography-based visual servo tracking control via a quaternion formulation. **IEEE Transactions on Control Systems Technology**, ., v. 18, n. 1, p. 128–135, 2009.

HUANG, Y.; JADBABAIE, A. Nonlinear H control: an enhanced quasi-lpv approach. **IFAC Proceedings Volumes**, ., v. 32, n. 2, p. 2754–2759, 1999.

KHALIL, H. K. **Nonlinear Systems**. 3. ed. New Jersey: Prentice Hall, 2002. 768 p.

KRISHNASWAMI, G. S.; SACHDEV, S. Algebra and geometry of Hamilton's quaternions. **Resonance**, ., v. 21, n. 6, p. 529–544, 2016.

KWIATKOWSKI, A.; BOLL, M.-T.; WERNER, H. Automated generation and assessment of affine LPV models. *In*: IEEE CONFERENCE ON DECISION AND CONTROL, 45., 2006, . **Proceedings [...]** Elsevier, 2006. p. 6690–6695.

LEE, T. Geometric tracking control of the attitude dynamics of a rigid body on SO(3). *In*: AMERICAN CONTROL CONFERENCE, 2011., 2011, . **Proceedings [...]** ., 2011. p. 1200–1205.

LOFBERG, J. YALMIP: a toolbox for modeling and optimization in matlab. *In*: IEEE INTERNATIONAL CONFERENCE ON ROBOTICS AND AUTOMATION (IEEE CAT. NO. 04CH37508), 2004., 2004, . **Proceedings [...]** IEEE, 2004. p. 284–289.

MA, Y. *et al.* **An Invitation to 3-D Vision**. .: Springer-Verlag, 2004.

MACKENROTH, U. **Robust Control Systems**. 1. ed. New York, US: Springer-Verlag Berlin Heidelberg, 2004.

MAHONY, R.; HAMEL, T. Image-based visual servo control of aerial robotic systems using linear image features. **IEEE Transactions on Robotics**, ., v. 21, n. 2, p. 227–239, 2005.

MARKLEY, F. L.; CRASSIDIS, J. L. **Fundamentals of spacecraft attitude determination and control**. .: Springer, 2014.

MAYHEW, C. G.; SANFELICE, R. G.; TEEL, A. R. On quaternion-based attitude control and the unwinding phenomenon. *In*: AMERICAN CONTROL CONFERENCE, 2011., 2011, . **Proceedings [...]** ., 2011. p. 299–304.

POLCZ, P.; SZEDERKÉNYI, G.; PÉNI, T. An improved method for estimating the domain of attraction of nonlinear systems containing rational functions. *In*: JOURNAL OF PHYSICS: CONFERENCE SERIES, 2015, Bristol, UK. **Proceedings [...]** IOP Publishing, 2015. v. 659, n. 1, p. 012038.

ROBLES, R.; SALA, A.; BERNAL, M. Performance-oriented quasi-LPV modeling of nonlinear systems. **International Journal of Robust and Nonlinear Control**, ., v. 29, n. 5, p. 1230–1248, 2019.

SADABADI, M. S.; PEAUCELLE, D. From static output feedback to structured robust static output feedback: a survey. **Annual reviews in control**, ., v. 42, p. 11–26, 2016.

SALTON, A. T. *et al.* Semidefinite programming solution to the spacecraft analysis and control problem. **IFAC-PapersOnLine**, ., v. 50, n. 1, p. 3959–3964, 2017.

SARAIVA, E. S. **Control design for robotic manipulator systems subject to saturating actuators**. 2019. Dissertação (Mestrado em Engenharia Elétrica) — Pontifícia Universidade Católica do Rio Grande do Sul, 2019.

SHAH, M. Fundamentals of computer vision. **Orlando: University of Central Florida**, ., 1997.

SPRING, K. W. Euler parameters and the use of quaternion algebra in the manipulation of finite rotations: a review. **Mechanism and machine theory**, ., v. 21, n. 5, p. 365–373, 1986.

TOKER, O.; OZBAY, H. On the NP-hardness of solving Bilinear Matrix Inequalities and simultaneous stabilization with static output feedback. *In*: AMERICAN CONTROL CONFERENCE-ACC'95, 1995., 1995, . **Proceedings [...]** ., 1995. v. 4, p. 2525–2526.

TROFINO, A. Robust stability and domain of attraction of uncertain nonlinear systems. *In*: AMERICAN CONTROL CONFERENCE. ACC (IEEE CAT. NO. 00CH36334), 2000., 2000, . **Proceedings [...]** ., 2000. v. 5, p. 3707–3711.

TROFINO, A.; DEZUO, T. LMI stability conditions for uncertain rational nonlinear systems. **International Journal of Robust and Nonlinear Control**, ., v. 24, n. 18, p. 3124–3169, 2014.